The nuclear basket proteins Mlp1p and Mlp2p are part of a dynamic interactome including Esc1p and the proteasome

Mario Niepel[a], Kelly R. Molloy[b], Rosemary Williams[c], Julia C. Farr[c], Anne C. Meinema[d,*], Nicholas Vecchietti[e,f], Ileana M. Cristea[b,†], Brian T. Chait[b], Michael P. Rout[c], and Caterina Strambio-De-Castillia[f]

[a]Department of Systems Biology, Harvard Medical School, Boston, MA 02115; [b]Laboratory of Mass Spectrometry and Gaseous Ion Chemistry and [c]Laboratory of Cellular and Structural Biology, Rockefeller University, New York, NY 10065; [d]Institute for Research in Biomedicine and [e]Istituto Cantonale di Microbiologia, 6500 Bellinzona, Switzerland; [f]Program in Molecular Medicine, University of Massachusetts Medical School, Worcester, MA 01605

ABSTRACT **The basket of the nuclear pore complex (NPC) is generally depicted as a discrete structure of eight protein filaments that protrude into the nucleoplasm and converge in a ring distal to the NPC. We show that the yeast proteins Mlp1p and Mlp2p are necessary components of the nuclear basket and that they also embed the NPC within a dynamic protein network, whose extended interactome includes the spindle organizer, silencing factors, the proteasome, and key components of messenger ribonucleoproteins (mRNPs). Ultrastructural observations indicate that the basket reduces chromatin crowding around the central transporter of the NPC and might function as a docking site for mRNP during nuclear export. In addition, we show that the Mlps contribute to NPC positioning, nuclear stability, and nuclear envelope morphology. Our results suggest that the Mlps are multifunctional proteins linking the nuclear transport channel to multiple macromolecular complexes involved in the regulation of gene expression and chromatin maintenance.**

Monitoring Editor
Karsten Weis
University of California, Berkeley

Received: Aug 8, 2013
Revised: Oct 16, 2013
Accepted: Oct 17, 2013

INTRODUCTION

Traffic across the nuclear envelope (NE), which separates the nucleus and cytoplasm, occurs through nuclear pore complexes (NPCs) located at circular apertures resulting from the fusion of the inner and outer nuclear membranes. Although the core function of the NPC is to regulate nucleocytoplasmic transport, a growing body of evidence suggests involvement in many other cellular activities, including epigenetic regulation of gene expression and chromatin maintenance (reviewed in Strambio-De-Castillia *et al.*, 2010; Bermejo *et al.*, 2012). A detailed map of the central structure of the yeast (*Saccharomyces cerevisiae*) NPC (Alber *et al.*, 2007a,b) revealed that it is composed of multiple copies of ~30 different proteins (nucleoporins [Nups]). Core scaffold Nups stabilize the nuclear pore membrane and form the central transport tube, and linker Nups bridge the scaffold to a dozen largely unfolded FG Nups, which in turn line the surface of the transporter and regulate nucleocytoplasmic transport. Even though the peripheral structures of the NPC, including the nuclear basket, were not represented in this map, a consensus view depicts the basket as a distal ring connected to the nuclear face of the NPC by eight ~60- to 80-nm-long proteinaceous filaments (Jarnik and Aebi, 1991; Goldberg and Allen, 1992). The basket appears to be a flexible structure that allows even large RNPs access to the central transporter via rearrangement of the distal ring during nuclear export (Kiseleva *et al.*, 1996, 1998). The basket might also contribute to the spatial organization of chromatin

This article was published online ahead of print in MBoC in Press (http://www.molbiolcell.org/cgi/doi/10.1091/mbc.E13-07-0412) on October 23, 2013.

Present addresses: *Groningen Biomolecular Sciences and Biotechnology Institute, Department of Biochemistry, University of Groningen, 9747 AG Groningen, Netherlands; †Department of Molecular Biology, Princeton University, Princeton, NJ 08544.

Address correspondence to: Caterina Strambio-De-Castillia (caterina.strambio@umassmed.edu), Michael P. Rout (rout@rockefeller.edu).

Abbreviations used: FRAP, fluorescence recovery after photobleaching; GFP, green fluorescent protein; IEM, immuno–electron microscopy; IF, immunofluorescence; MFI, mean fluorescence intensity; Mlp, myosin-like protein; mRNP, messenger ribonucleoprotein; MS, mass spectrometry; NBS, nuclear pore complex–binding site; NE, nuclear envelope; NLS, nuclear localization sequence; NPC, nuclear pore complex; Nup, nucleoporin; PrA, protein A; SEM, standard error of the mean; SPB, spindle pole body; TEM, transmission electron microscopy; Tpr, translocated promoter region.

by selectively excluding unwanted macromolecular assemblies such as heterochromatin or large RNPs (Krull *et al.*, 2010; Kylberg *et al.*, 2010) from the vicinity of the NPC entrance while also mooring actively transcribed chromatin to it (Ishii *et al.*, 2002; Casolari *et al.*, 2004; Dilworth *et al.*, 2005; Taddei *et al.*, 2006; Luthra *et al.*, 2007).

In metazoans, the inner nuclear membrane is lined by the nuclear lamina (reviewed in Andres and Gonzalez, 2009), an extensive network of lamins and other proteins that underlies and supports the NE in close connection with distal NPC structures (Daigle *et al.*, 2001; Zhou and Pante, 2010). In the amphibians *Xenopus* and *Triturus*, the outer rings of the nuclear basket are interconnected to form a NE lattice composed of 8- to 10-nm-diameter fibrils whose molecular composition is unknown (Goldberg and Allen, 1992; Ris, 1997; Arlucea *et al.*, 1998). Although yeast lack lamins, they contain similar structures, suggesting that these basket projections might be a conserved feature of eukaryotes (Kiseleva *et al.*, 2004).

The translocated promoter region (Tpr) protein (Cordes *et al.*, 1997; Bangs *et al.*, 1998) constitutes the central scaffold of the vertebrate basket (Krull *et al.*, 2004; Soop *et al.*, 2005). Only one gene encodes Tpr in vertebrates. Conversely, yeasts *S. cerevisiae* and *Schizosaccharomyces pombe* and the trypanosome *Trypanosoma brucei* may express two similar but functionally distinct Tpr homologues (Ding *et al.*, 2000; Kuznetsov *et al.*, 2002; DeGrasse *et al.*, 2009). The *S. cerevisiae* homologues, myosin-like protein 1 (Mlp1p; Kölling *et al.*, 1993) and Mlp2p, are large proteins (~200 kDa) predicted to have an extended filamentous N-terminal coiled-coil–rich domain and a C-terminal head of undetermined structure (Strambio-de-Castillia *et al.*, 1999). Even though the Mlps are not part of the NPC core structure, a significant fraction of Mlp molecules colocalizes with those NPCs that are excluded from regions of the NE underlying the nucleolus (Strambio-de-Castillia *et al.*, 1999; Galy *et al.*, 2004; Niepel *et al.*, 2005). On the other hand, immuno–electron microscopy (IEM) demonstrates that only a subset of the Mlps are found directly at the NPC at any one time, with the remainder located either in inter-NPC regions at the NE or at the nuclear interior (Strambio-de-Castillia *et al.*, 1999; Kosova *et al.*, 2000). An array of NE-associated functions has been proposed for the Mlp/Tpr family members: transcriptional regulation (Vinciguerra *et al.*, 2005; Cabal *et al.*, 2006; Tan-Wong *et al.*, 2009; Vaquerizas *et al.*, 2010), RNA biogenesis (Green *et al.*, 2003; Galy *et al.*, 2004; Vinciguerra *et al.*, 2005; Iglesias *et al.*, 2010; Rajanala and Nandicoori, 2012; Sayani and Chanfreau, 2012), SUMO homeostasis (Zhao *et al.*, 2004; Palancade *et al.*, 2007; Xu *et al.*, 2007), chromatin organization (Feuerbach *et al.*, 2002; Hediger *et al.*, 2002; Bermejo *et al.*, 2011), proliferation, and senescence (Niepel *et al.*, 2005; Scott *et al.*, 2005; Lince-Faria *et al.*, 2009; Nakano *et al.*, 2010; David-Watine, 2011; Ding *et al.*, 2012; Funasaka *et al.*, 2012).

Here we establish that the Mlp proteins are major and necessary components of the NPC basket and show data consistent with a model positing that the Mlps are part of a dynamic protein network that interconnects neighboring NPCs. We present evidence linking this network with the NE-associated protein Esc1p and, through it, silencing factors and the proteasome. We show that the Mlps influence NPC positioning and are critical for the structure, integrity, and function of the NE and the nucleus. Taken together, the data presented here tie together a host of phenotypic observations related to the Mlps that to this date have not received a satisfactory molecular explanation.

RESULTS

Mlps interact extensively with NPCs and mRNA transport machinery

Affinity purification of protein A (PrA)–tagged Mlp1p and Mlp2p in increasingly stringent extraction buffers, and subsequent mass spectrometry (MS) analysis of coenriching proteins visible by Coomassie blue staining (Figure 1, A and B, and Supplemental Table S1), show that both Mlps are in complex with nuclear transport factors, components of the mRNA processing machinery, and a significant subset of Nups; Mlp2p is also associated with the yeast spindle pole body (SPB; Niepel *et al.*, 2005). Using a rapid and mild isolation protocol intended to preserve low-affinity and dynamic interactions (Oeffinger *et al.*, 2007), we found Mlp1p-PrA and Mlp2p-PrA predominantly in complex with Nups that form the peripheral scaffold and inner transport channel of the yeast NPC (Figure 1, C and D, and Supplemental Table S2), a subset of which were previously identified in complex with the Mlps (Scott *et al.*, 2005). Mlp1p is also found in complex with multiple essential components of the machinery linking transcription and mRNA export (Yra1p, Mex67p, and TREX-2 components Sac3p, Thp1p, and Cdc31p; Jani *et al.*, 2012), whereas Mlp2p is found only in complex with Mex67p. Both Mlps cofractionate with members of the Nup84p complex and Nup1p, but only Mlp1p was found in complex with the peripheral nucleoporin Nup60p, consistent with prior findings (Galy *et al.*, 2000; Feuerbach *et al.*, 2002; Scott *et al.*, 2005; Lewis *et al.*, 2007). These observations indicate that the Mlps are tethered to one or more Nups at the nuclear face of the NPC, which in turn bridge interactions with the other copurifying Nups.

To identify Mlp anchoring points at the NPC, we generated deletion strains for key components of each of the NPC substructures and analyzed both the resulting Mlp-containing complexes and Mlp localization in these strains. Deletion of Nup60p completely abrogated Mlp1p attachment to the NPC (Figure 2A and Supplemental Table S3), as was further confirmed by a hypothesis-driven MS/MS analysis (Kalkum *et al.*, 2003) targeted to identify Nups (unpublished data). Immunofluorescence (IF) microscopy confirmed that in the absence of Nup60p, Mlp1p localizes to peripheral nuclear foci rather than the NE (Figure 3A), consistent with published observations (Feuerbach *et al.*, 2002; Galy *et al.*, 2004; Lewis *et al.*, 2007). Similarly, deletion of Nup1p caused mislocalization of Mlp1-PrA to the cytoplasm and largely abrogated Nup binding, although trace amounts of some Nups remained associated with Mlp1p, making them candidate anchor sites (Figure 2A and Supplemental Table S3). Comparable results were obtained for deletion of the outer ring component Nup84p (Figure 2A and Supplemental Table S3). Mlp2p localization and Nup association were also highly sensitive to deletion of those same three proteins (Figures 2B and 3B and Supplemental Table S4). As we observed with Mlp1p, Nsp1p and the linker Nic96p remain associated with Mlp2p in trace amounts in some of deletion strains and are therefore also possible anchor sites (Kosova *et al.*, 2000). We also deleted components of either the inner ring (Nup188p, Nup53p) or the transmembrane ring (Pom152p). Mlp1-PrA association with the NPC appears to be fully maintained in these deletions (Figures 2C and 3C and Supplemental Table S5). These observations suggest that the Mlps anchor at the NPC via multiple interactions that involve at least the outer ring on the nuclear face of the NPC and the nuclear FG Nups, Nup1p and Nup60p.

Even though earlier work indicated that Mlp1p and Mlp2p might interact directly (Niepel *et al.*, 2005; Palancade *et al.*, 2005), this interaction was abolished in some Nup deletion strains (Figure 2), suggesting that assembly at the NPC might be required for these two proteins to associate. We performed coimmunoprecipitation followed by immunoblotting, using PrA-tagged Mlps as bait and

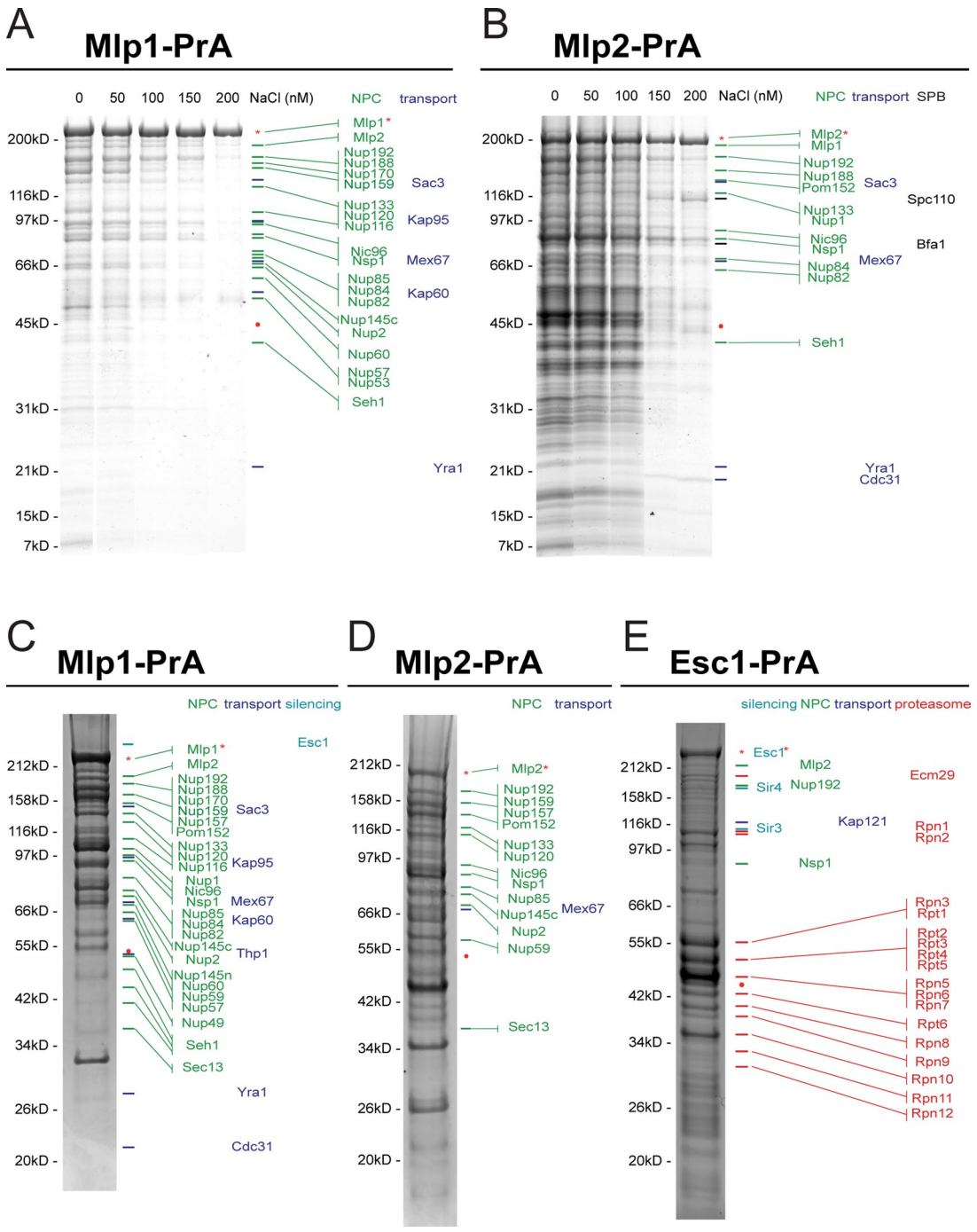

FIGURE 1: Mlp1p, Mlp2p, and Esc1p participate in a network of interactions at NPCs that includes transport and silencing factors, the proteasome, and the SPB. (A, B) PrA-containing complexes from strains expressing Mlp1p-PrA (A) or Mlp2p-PrA (B) were affinity purified at increasing NaCl concentration, and protein composition was determined by MS. (C–E) Proteins in complex with Mlp1p-PrA (C), Mlp2p-PrA (D), or Esc1-PrA (E) were affinity purified via a mild isolation protocol and identified by MS. (Identified proteins are listed to the right of each gel image and in Supplemental Tables S1 (A, B) and S2 (C–E). Red asterisks indicate PrA-tag bait, and red circles indicate IgG heavy chain.

Myc-tagged Mlps as targets (Figure 4), and found that in coexpressing strains, Mlp1p-PrA or Mlp2p-PrA bound both Myc-tagged Mlps (Figure 4, A and B, coexpressed). This interaction did not occur when we mixed lysates from cells expressing the two proteins separately, demonstrating that the interaction required a physiologically relevant assembly process and does not occur postlysis (Figure 4, A and B, mixed). We also note that smaller amounts of Mlp2p-Myc purified with the PrA-tagged bait than Mlp1p-Myc, consistent with Mlp1p forming a more extensive and coherent structure at the nuclear periphery than Mlp2p (Niepel *et al.*, 2005).

Esc1p and the proteasome are part of the extended Mlp interactome

The Mlp1p complex also contained notable amounts of Esc1p (Figure 1C), a peripheral nuclear protein involved in telomere silencing, NE structural organization, SUMO-dependent mRNA

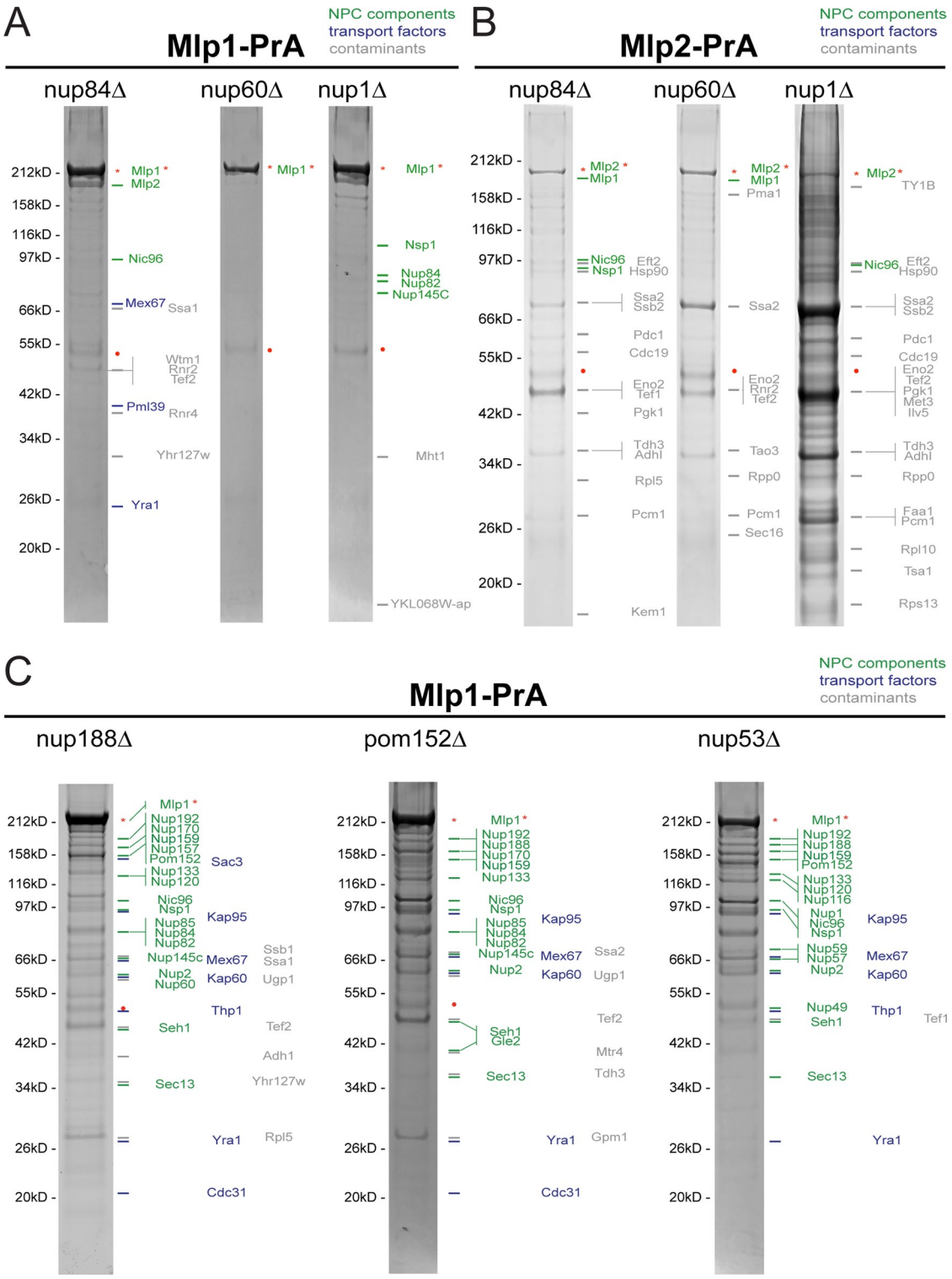

FIGURE 2: Peripheral nuclear Nups and Nup84p serve as NPC-anchoring partners for the Mlps, whereas structural and membrane Nups do not. (A, C) Mlp1p-PrA- and (B) Mlp2p-PrA-containing complexes were affinity purified from *nup84Δ*, *nup60Δ*, and *nup1Δ* or from *nup188Δ*, *pom152Δ*, and *nup53Δ* strains using IgG-conjugated magnetic beads, and Mlp-interacting proteins were identified by MS as described in Figure 1, C–E. Identified proteins, as well as known affinity purification contaminants, are indicated at right and in Supplemental Tables S3–S5. Red asterisks and red circles, respectively, indicate PrA bait and IgG.

proofreading, and DNA repair (Andrulis *et al.*, 2002; Taddei *et al.*, 2004; Hattier *et al.*, 2007; Lewis *et al.*, 2007; Skruzný *et al.*, 2009; Pasupala *et al.*, 2012), which was not previously known to interact with Mlps. We affinity purified PrA-tagged Esc1p (Figure 1E and Supplemental Table S2) and identified Sir3 and Sir4 as part of its interacting complex, consistent with previous reports

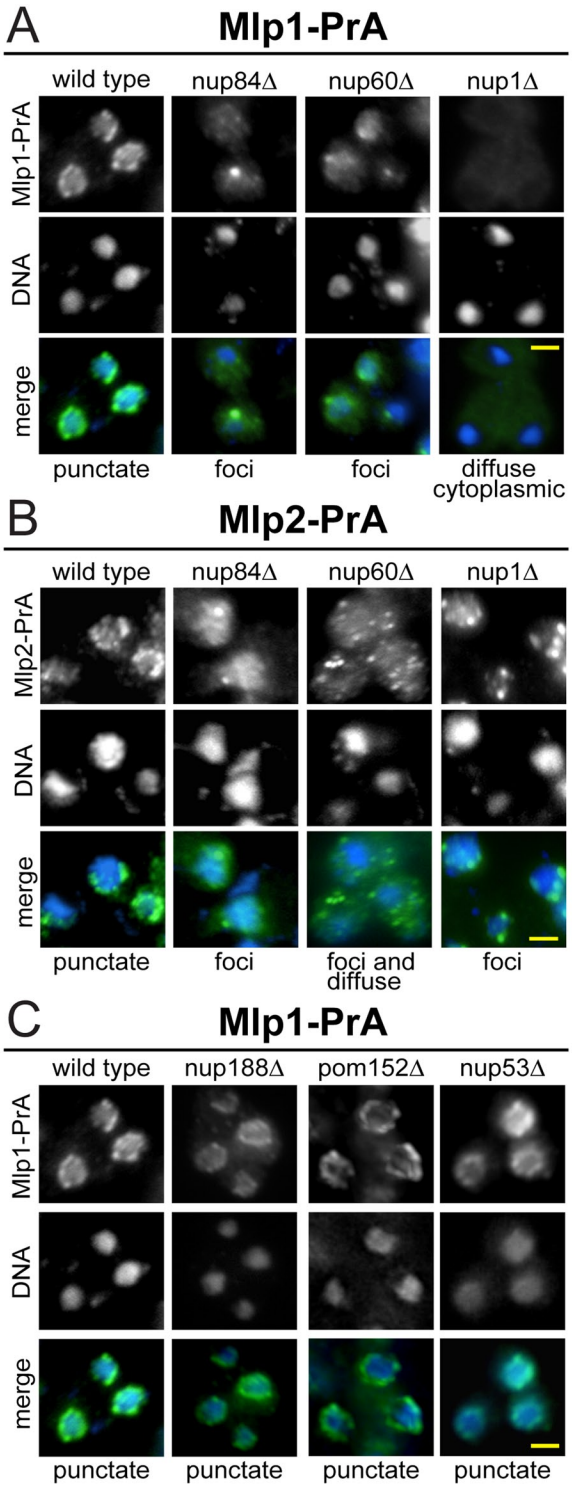

FIGURE 3: The Mlps miscolocalize in the absence of peripheral nuclear Nups and Nup84p but not of structural and membrane Nups. Wild-type and Nup-deletion strains expressing (A, C) Mlp1p-PrA or (B) Mlp2p-PrA were imaged by IF to reveal the position of the PrA tag and counterstained with DAPI to reveal the position of the nucleus. Shown are single-plane images of the tagged Mlp proteins (top), DNA (middle), and an overlay of the two (bottom). (A, B) Mlp1p-PrA and Mlp2p-PrA lose their association with the NPC in the absence of the indicated peripheral nuclear Nups and either appear diffuse or have a focal pattern. (C) Mlp1p-PrA maintains a characteristic punctate rim-staining pattern, indicating association with the NPC, in the absence of the indicated scaffolding and membrane-associated Nups. Bars, 2 μm.

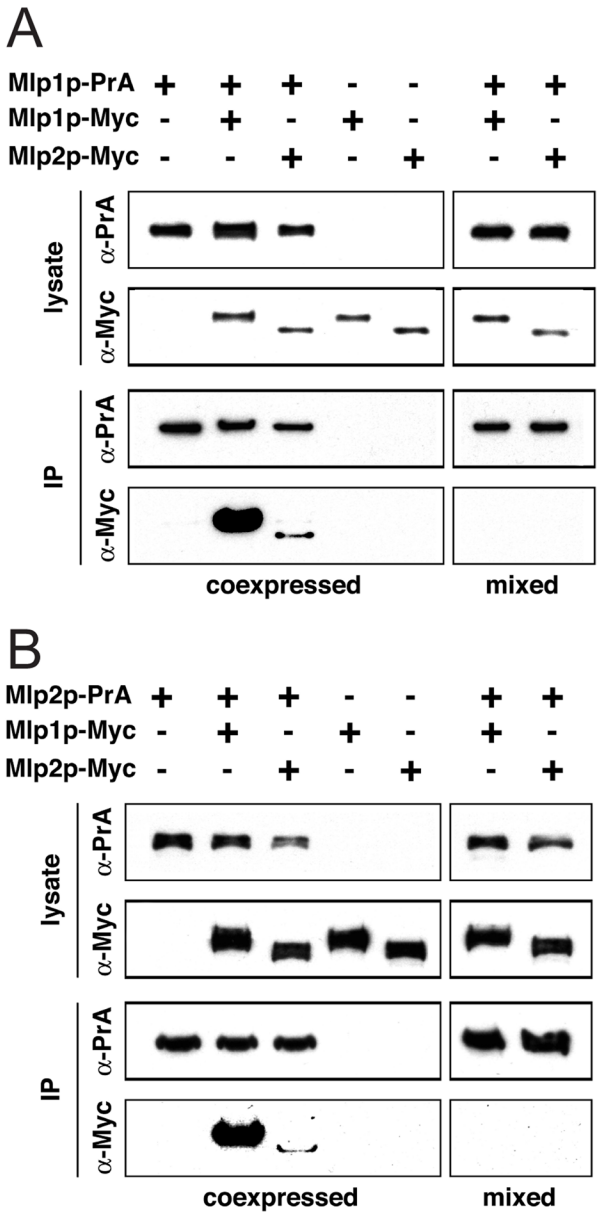

FIGURE 4: Mlp1p and Mlp2p form homomeric and heteromeric interactions ex vivo but not when mixed in vitro. PrA-containing affinity-purified complexes (IP) and whole-cell lysates (lysate) of strains coexpressing combinations of (A) Mlp1p-PrA or (B) Mlp2p-PrA as baits and Myc-tagged Mlp1p or Mlp2p as targets were probed by immunoblotting for Myc and PrA (coexpressed). To control for interactions occurring postlysis, strains expressing either one PrA-tagged bait or one Myc-tagged target were mixed after cell lysis and analyzed as described (mixed).

(Andrulis *et al.*, 2002). We also identified Mlp2p and two nucleoporins (Nup192p and Nsp1p), confirming the participation of Esc1p in the Mlp-NPC interactome. Given that these components are present only in substoichiometric amounts, it is likely that only a small amount of Esc1p takes part in this interaction, suggesting a transient or indirect interaction. We also found Esc1p in complex with Kap121p, which might be involved in its nuclear import.

We investigated the position of Esc1p and the Mlps relative to the NPC by IF (Figure 5A). Both the Mlps and Esc1p predominantly localized to C-shaped peripheral nuclear regions that were previously shown to be excluded from the nucleolus and to only partially

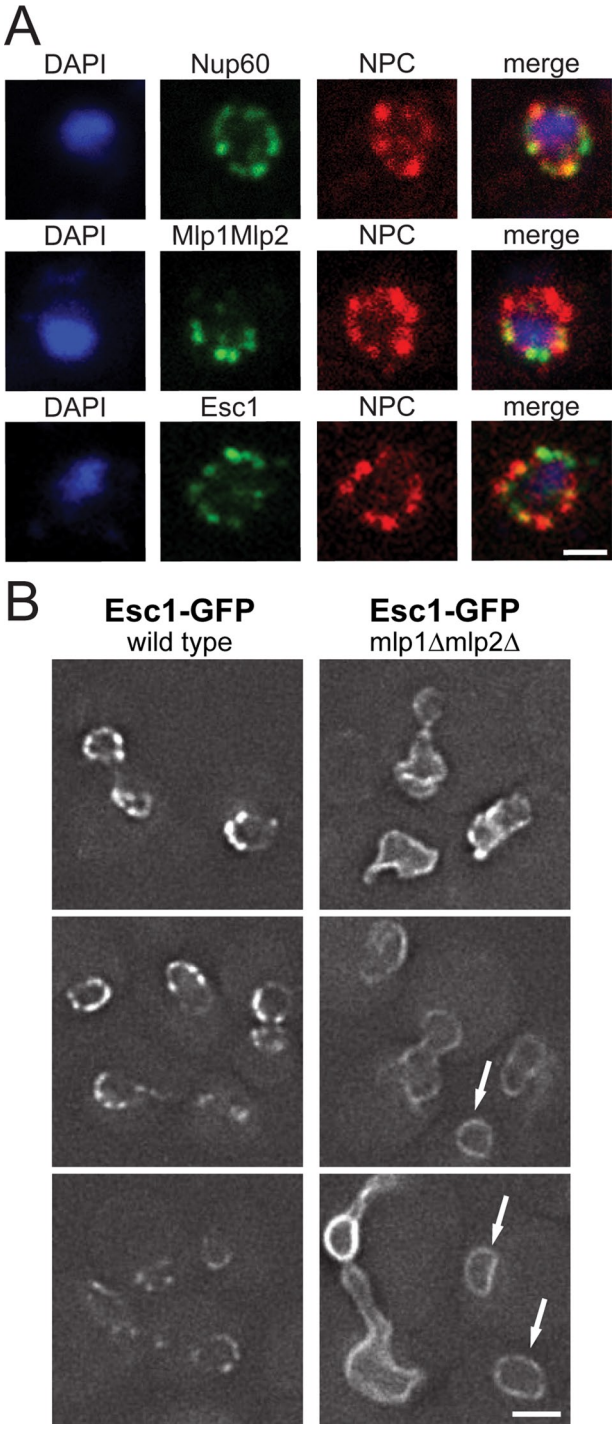

FIGURE 5: Esc1p and the Mlps show similar localization at the NE, and Esc1p requires Mlps for normal localization. (A) Pseudocolored IF images of cells expressing GFP-tagged Nup60p, Mlp1p and Mlp2p, or Esc1p, stained for GFP, the NPC (MAb414), and DNA. (B) Fluorescence microscopy images of cells derived from three different pairs of sister spores expressing Esc1p-GFP in wild-type or *mlp1Δmlp2Δ* cells. Nuclei with normal morphology in *mlp1Δmlp2Δ* cells are marked with white arrows. Differences in Esc1p-GFP brightness reflect natural variation of protein expression and localization in this mixed-strain background. Bars, 2 μm (A, B).

colocalize with NPCs (Strambio-de-Castillia *et al.*, 1999; Galy *et al.*, 2004; Taddei *et al.*, 2004; Niepel *et al.*, 2005). As a control, we compared the localization of Nup60p, which displayed a characteristic punctate rim staining that overlapped with the NPC and occupied the entire nuclear surface. These results indicate that Esc1p and the Mlps occupy similar locales at the nuclear rim, which are not exclusively associated with NPCs and are excluded from the nucleolus (Galy *et al.*, 2004; Taddei *et al.*, 2004). Because we found that the Mlps and Esc1p interact (directly or indirectly), we tested whether Mlp proteins are necessary for proper localization of Esc1p–green fluorescent protein (GFP; Figure 5B). In contrast to the wild-type distribution (Taddei *et al.*, 2004), when both Mlp1p and Mlp2p are absent the Esc1p signal is much more broadly and evenly distributed around the entire NE and no longer appears to be sequestered from nucleolar regions. Although a subset of *mlp1Δmlp2Δ* cells have marked NE alterations, cells with seemingly normal nuclei (Figure 5B, white arrows) also display evenly distributed Esc1p-GFP.

To our surprise, the majority of proteins in complex with Esc1p were components of the proteasome. We identified nearly all the protein components of both the base and lid of the proteasome, as well as Ecm29p, which links these structures to the proteasome core (reviewed in Wolf and Hilt, 2004). These results suggest that the proteasome is linked via its regulatory subunit to Esc1p at the NE and that the proteasome is thus indirectly connected to the Mlp-NPC interactome. Previously published fluorescence microscopy studies suggested that the proteasome can localize to the NE under specific conditions (Enenkel *et al.*, 1998, 1999), and our results provide an explanation of how these two structures might be linked. Furthermore, our results offer the first biochemical evidence supporting models (reviewed in Nagai *et al.*, 2011) that call for the localization of the proteasome to the nuclear periphery to promote chromatin remodeling. This in turn could contribute to spatial regulation of transcriptional activity (Faza *et al.*, 2009, 2010), mRNA surveillance (Saguez *et al.*, 2008; Wilmes *et al.*, 2008), double-stranded DNA break repair (Krogan *et al.*, 2004), and maintenance of NE structure (Titus *et al.*, 2010).

A hinge region of Mlp forms the NPC-binding site

To identify the Mlp1p nuclear pore complex–binding site (NBS), we fused fragments of its open reading frame that were large enough to homodimerize (Hase *et al.*, 2001) to GFP and a nuclear localization sequence (NLS). Only the N-term 2 fragment (amino acids 338–616) showed the punctate rim pattern typical of NPC-associated proteins and displayed peak intensity at the NE, suggesting that this region is sufficient for anchoring Mlp1p to the NE (Figure 6A). All other fragments exhibited diffuse nuclear staining with no enrichment at the NE. We confirmed this result by IF and found that the signal associated with the N-term 2 fragment partially overlaps with the NPC on the inner face of the NE (Figure 6B), similar to what was observed upon Mlp1p overexpression (Strambio-de-Castillia *et al.*, 1999). The majority of Mlp1p's amino acid sequence is predicted to fold into a coiled coil (Kölling *et al.*, 1993; Strambio-de-Castillia *et al.*, 1999), but analysis with the PARCOIL algorithm (Lupas, 1997) suggests that the segment corresponding to the N-term 2 fragment contains a major region of coiled-coil discontinuity (Figure 6C), which we verified by protease accessibility laddering (PAL) experiments (Supplemental Figure S1 and Supplemental Table S6; Dokudovskaya *et al.*, 2006). This algorithm found other regions of discontinuity in both Mlps that were also supported by PAL (Supplemental Figure S1), indicating that the N-terminal regions of these proteins might not form rigid rods but instead resemble "beads on a string," with discrete coiled-coil segments separated by short, flexible regions. Unlike full-length Mlp1p, the N-term 2 fragment appears to interact with the entire NE, suggesting that Mlp exclusion from nucleolar areas is due to a mechanism other than NPC compositional heterogeneity.

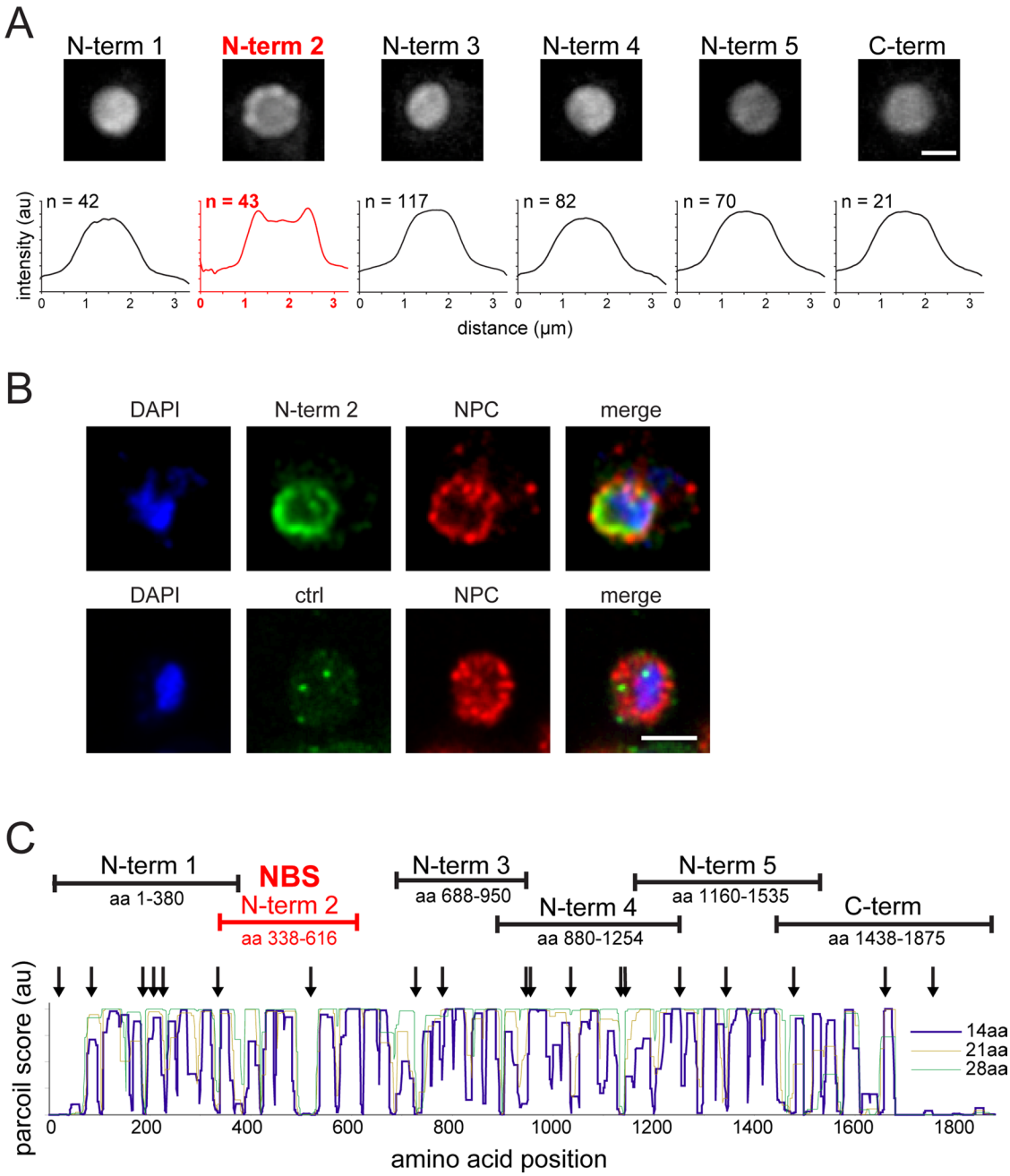

FIGURE 6: Mlp1p is attached to the NPC via a binding domain within a flexible region of the coiled-coil domain. (A) Live fluorescence images of cells expressing GFP-NLS fusion proteins of Mlp1p fragments and plots of the average MFI along the nuclear diameter (*n*, number of images analyzed). (B) IF images of cells expressing either GFP-NLS tagged N-term 2 or a GFP-NLS control stained for GFP and the NPC (MAb414). (C) PARCOIL score predictions along Mlp1p, calculated using 14–, 21–, or 28–amino acid sliding windows. Sites of preferential protease cleavage (Supplemental Figure S1) are indicated by vertical arrows. Bar, 2 µm (A).

Mlp proteins are major components of the NPC nuclear basket

We investigated the position of both PrA-tagged N- and C-termini of Mlp1p and of Mlp2p with respect to the NPC central structure by pre-embedding IEM mapping, as previously described (Figure 7, A–C; Alber *et al.*, 2007a). We found that the N- and C-termini of both Mlps localize up to 60 nm into the nucleus, as measured from the midplane of the NE. Because both ends are located further from the NPC than even the most peripheral Nup and the Mlp1p NBS is in a central region of the protein (Figure 6C), the Mlp proteins are likely anchored to the NPC in a hairpin-loop conformation, as previously suggested for vertebrate Tpr (Krull *et al.*, 2004). Mlp proteins are not found exclusively at the NPC (Strambio-de-Castillia *et al.*, 1999), so we also estimated the position of N- and C-termini for Mlps in regions of the NE that lie away from discernible NPCs (Figure 7, D–F). The ends of both Mlps localized 30–40 nm away from the midplane of the NE, but unlike at the NPC, there were no clear differences in localization between Mlp1p and Mlp2p. This suggests that Mlps not directly associated with NPCs assume a horizontal arrangement underneath the NE, since the greater length of Mlp1p

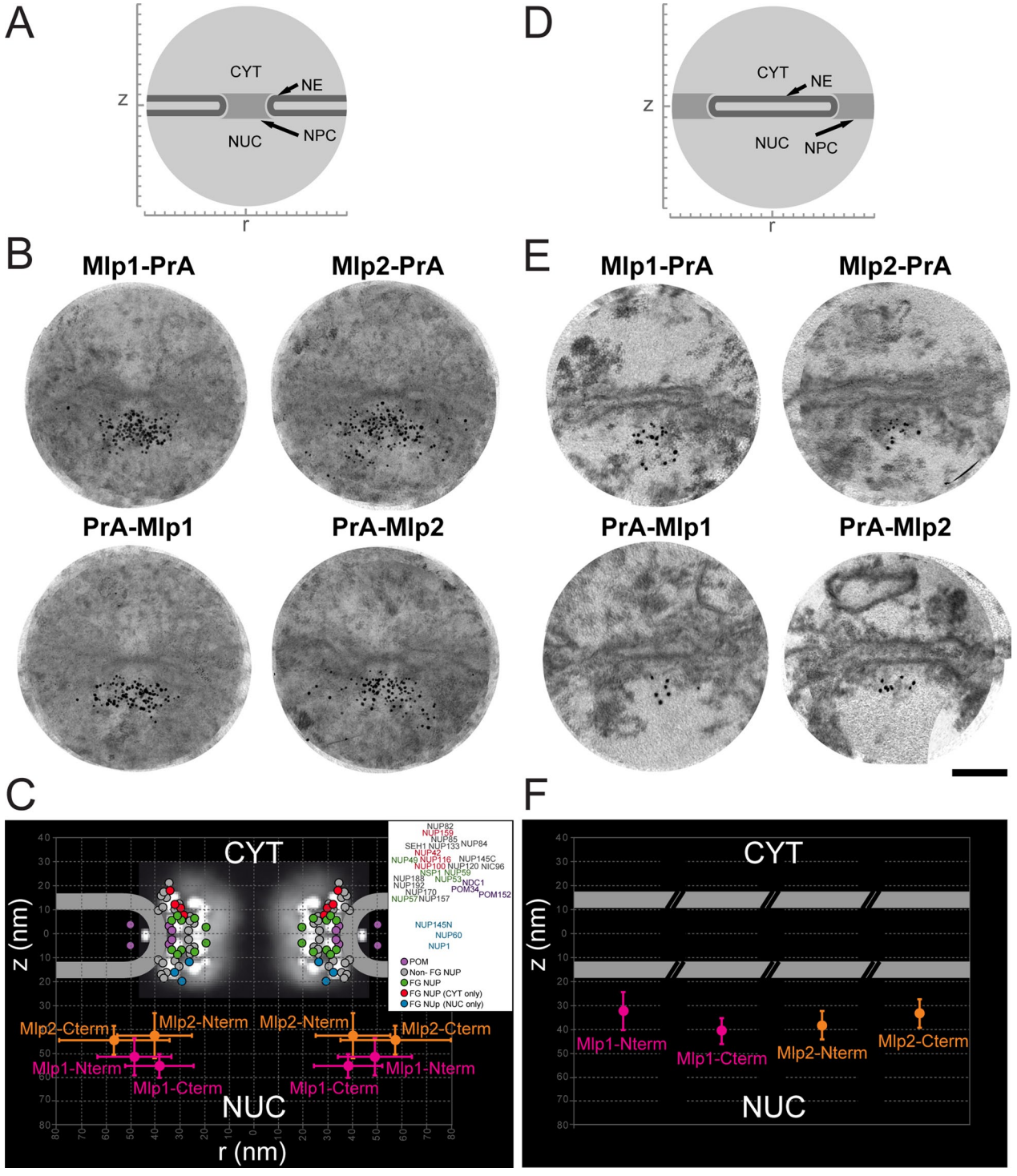

FIGURE 7: Mlp proteins localize to the NPC basket and to inter-NPC regions of the NE. Schematic depiction of (A) the NPC and (D) the area between NPCs. (B, E) Overlays of multiple IEM images with gold-labeled antibodies bound to the C- (top) and N-termini (bottom) of either Mlp1p (left) or Mlp2p (right), showing circular zones (diameter, 400 nm) around (B) visible NPCs or (E) regions between NPCs. (C, F) Extracted *z*- and *r*-positions of the N- and C-termini of Mlp1p and Mlp2p in relation to the (C) NPC or (F) NE in inter-NPC regions. (C) Mlp1p-PrA, $n = 210$; Mlp2p-PrA, $n = 210$; PrA-Mlp1, $n = 122$; PrA-Mlp2, $n = 121$. (F) Mlp1p-PrA, $n = 244$; Mlp2p-PrA, $n = 152$; PrA-Mlp1, $n = 127$; PrA-Mlp2, $n = 153$. Bar, 100 nm (B, E).

does not lead to a greater distance from the midplane of the NE than Mlp2p.

Because our standard NE preparation technique is not suited to preserve the morphology of peripheral structures of the NPC, we developed a novel method for rapid isolation and EM visualization of yeast nuclei that allowed us to observe the basket structure. Nuclei isolated from wild-type cells appeared to be well preserved, and we observed numerous NPCs with protein structures corresponding to nuclear baskets, which were notably absent in nuclei from *mlp1Δmlp2Δ* cells (Figure 8A). Insets show magnified individual

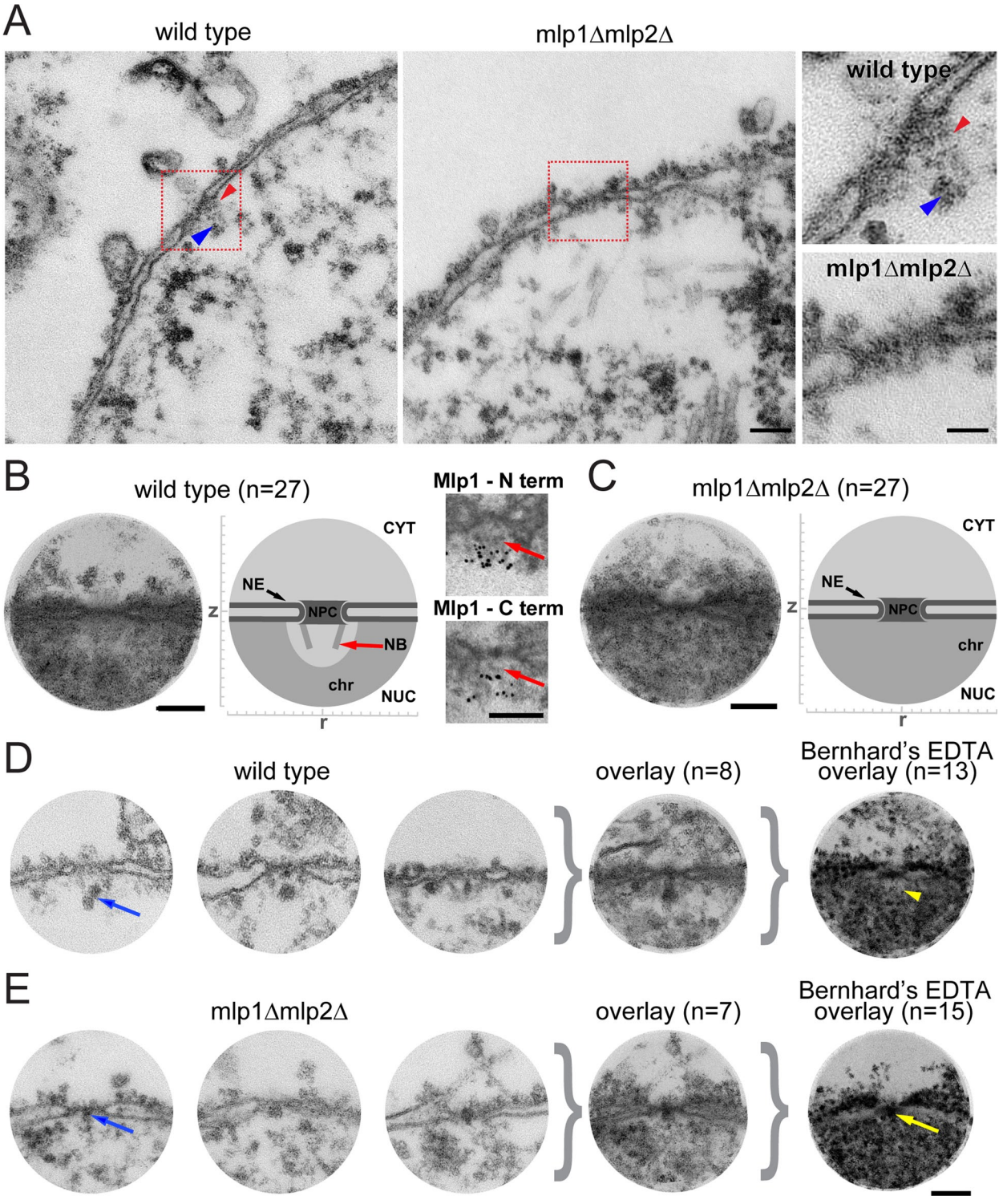

FIGURE 8: Mlp filaments form the NPC basket and keep the central tube free from mRNPs and chromatin. (A) TEM images of isolated nuclei from wild-type cells show the NPC-associated nuclear basket (red arrowheads), which is absent in *mlp1Δmlp2Δ* cells. Insets show individual NPCs at higher magnification. Electron-dense particles at the basket are highlighted (blue arrowhead). (B, C) Overlays of multiple electron micrographs (diameter, 400 nm) showing that the NPC is kept clear of chromatin by the basket in wild-type but not in *mlp1Δmlp2Δ* cells. Insets, overlays of four gold-labeled IEM images showing that Mlp1p is a major component of the basket (red arrows). (D, E) Micrographs of three individual NPCs (left) and of multiple overlaid NPCs (overlay), with electron-dense particles binding to or traversing through NPCs in (D) wild-type and (E) *mlp1Δmlp2Δ* cells. Overlays of Bernhard's EDTA-stained images (Bernhard's EDTA overlay) show that the electron-dense particles are largely composed of RNA. In wild-type cells they appear to be kept clear of the NPC central transporter (yellow arrowhead), whereas in the *mlp1Δmlp2Δ* strain they appear to cover it (yellow arrow). Bars, 100 nm (A–E), 40 nm (A, inset).

NPCs and underscore the absence of filamentous structures associated with the nuclear face of the NPC in *mlp1Δmlp2Δ* cells. The highlighted electron-dense structures found in proximity to the basket in wild-type cells are presumably RNP particles (see also later discussion) bound to the NPC (Figure 8A, blue arrowheads). Composite images of roughly 30 NPCs from wild type (Figure 8B) reveal a pattern closely matching the reported size and structure of the putative yeast basket (Rout and Blobel, 1993; Fahrenkrog *et al.*, 1998; Kiseleva *et al.*, 2004) and corresponding in size and location to the inferred position of the Mlps (Figure 7C). We found no filaments projecting from the nuclear face of the NPC in similar composites from the *mlp1Δmlp2Δ* strain, further indicating that Mlp proteins are necessary to form the nuclear basket structure. Previous ultrastructural observation of Mlp1p both in vivo (Strambio-de-Castillia *et al.*, 1999; Kosova *et al.*, 2000) and in vitro (Kosova *et al.*, 2000) showed that Mlp1p can form thin filaments. To further confirm that the Mlp proteins are part of the basket structure, we performed IEM staining on nuclei from strains expressing Mlp1p tagged with PrA at either the N- or C-terminus, as described for Figure 7. The insets show gold-labeled filaments in the area of the basket (Figure 8B, red arrows).

The Mlp basket reduces chromatin crowding and aids messenger ribonucleoprotein transit

EM images from our rapid nuclear preparation technique show that the region underlying NPCs in wild-type strains appears to contain fewer electron-dense regions of chromatin than inter-NPC regions of the NE (Figure 8B). In contrast, in strains lacking both Mlps, the NPC nuclear face appears to be covered by electron-dense chromatin (Figure 8C), suggesting that the basket excludes or prevents the formation of packed chromatin in the area directly underlying the NPC. We also observed electron-dense granules in association with several NPCs (Figure 8, A, blue arrowhead, and D and E, blue arrows). In wild-type nuclei, these particles often appeared to be attached to extended Mlp filaments (Figure 8, A, red arrowhead, and B, red arrows), whereas others were closer to the NPC or even seemed to be traversing it (Figure 8D, blue arrows). In the *mlp1Δmlp2Δ* strain, these particles were frequently found within the NPC transporter, which became particularly obvious in montages of multiple NPCs (Figure 8E, blue arrows). We used Bernhard's EDTA regressive staining technique, which differentially contrasts RNA-containing structures (Bernhard, 1969), to confirm that these electron-dense particles contain RNA and likely represent RNPs caught en route from the nucleus to the cytoplasm (Figure 8, D and E, right, and Supplemental Figure S2).

Mlp proteins regulate NPC mobility and distribution

Owing to their interaction with the NPCs, their ability to homodimerize and heterodimerize, and their horizontal localization at the NE, Mlps could modulate NPC mobility, analogous to the lamina in mammalian cells (Daigle *et al.*, 2001). To test this hypothesis, we compared fluorescence recovery after photobleaching (FRAP) in wild-type versus *mlp1Δmlp2Δ* strains expressing Nup49p-GFP–labeled NPCs (Figure 9, A–D, and Supplemental Videos S1–S4). In wild-type cells, the average t_{50} was ~56 s, whereas NPCs became significantly more mobile in the absence of Mlp proteins, with t_{50} reduced by >50% (~23 s). In both strains, we observed that recovery appears to occur via lateral invasion of NPC clusters into the bleached area (Figure 9, A–D, yellow arrowheads), and previous work showed that the recovery of NPC-associated fluorescence occurs at a much faster rate than free Nup49p-GFP turnover at the NPC (Belgareh and Doye, 1997; Bucci and Wente, 1997).

We also compared the mobility of the Mlps relative to that of the NPCs (Figure 9 and Supplemental Video S5). In strains expressing both Mlp1p-GFP and Mlp2p-GFP, fluorescence recovery was extremely rapid (Figure 9, E and F; $t_{50} \approx 12$ s)—more than four times as fast as with Nup49p-GFP in wild type (Figure 9, A and B; $t_{50} \approx 56$ s). Whereas fluorescence recovery appears to occur mostly by lateral diffusion along the NE, presumably representing the movement of Mlp molecules bound to the NPC, the discontinuity of the fluorescence signal in both bleached and unbleached regions of the nuclear rim suggests that a considerable fraction of recovery might utilize a different mechanism. The existence of this dual recovery mechanism is underscored when we compare the distribution of the standard error of the mean (SEM) of the measured MFI for each time point across the three different strains. Whereas fluorescence associated with Nup49-GFP in wild type displays relatively little variability, this variability is higher in the *mlp1Δmlp2Δ* background (analysis of variance [ANOVA], $p < 0.0001$). This difference is further amplified in the Mlp1p-GFP, Mlp2p-GFP strain, for which the mean SEM of the fluorescence signal has a greater amplitude and larger variance than that displayed by the two preceding strains (ANOVA, $p < 0.0001$; Figure 9G).

We also measured the uniformity of NPCs distribution around the nuclear surface (Figure 9H) in both wild-type and *mlp1Δmlp2Δ* strains by quantifying the frequency of NPC-fluorescence foci brighter than the overall mean fluorescence intensity (MFI) of the NE. In this assay, the aggregation rate will be low if NPCs are distributed evenly on the NE surface. Conversely, it will be high if there are relatively many bright NPC clusters (Figure 9H). Wild-type cells showed an aggregation rate of 16 ± 3.4% whereas the *mlp1Δmlp2Δ* strain exhibited a significantly higher rate of 23 ± 4.6% ($p < 10^{-7}$, Student's *t* tests). This suggests that Mlp proteins are critical not only for normal motility, but also for even distribution of NPCs around the nuclear surface, either directly or indirectly.

Mlps contribute to nuclear and NE integrity

Previous studies suggested that abnormal NPC distribution detrimentally affects both NE structure and overall cellular fitness in *S. cerevisiae* (Wente and Blobel, 1994). In addition, NE-associated proteins have been implicated in the control of nuclear shape and in the prevention of gross NE abnormalities (Campbell *et al.*, 2006; Hattier *et al.*, 2007; Witkin *et al.*, 2010; Yewdell *et al.*, 2011). Thus it is plausible that through their interaction with the NPCs, the Mlps also help to maintain the structural integrity of the NE and nucleus. Nup49p-GFP labeling revealed that the NE in wild-type yeast cells forms a smooth, even surface, whereas some nuclei in the Mlp double-deletion strain exhibit blebbing—the formation of irregular bulges in the NE (Figure 10A, red arrow)—similar to phenotypes observed in NPC-clustering strains (Wente and Blobel, 1994), and *spo7* or *esc1* mutants (Campbell *et al.*, 2006; Hattier *et al.*, 2007; Witkin *et al.*, 2010; Yewdell *et al.*, 2011). Twenty-seven percent of *mlpΔ1mlp2Δ* nuclei had one or more blebs in their NE, whereas blebbing occurred rarely in wild-type nuclei (5.5%; Figure 10B). We also quantified nuclear shape differences for the two strains. Wild-type nuclei were mainly circular, whereas the majority of mutant nuclei were oval or irregularly shaped (Figure 10C). EM visualization of thin sections of whole yeast cells confirmed these results (Figure 10D). Wild-type nuclei looked round, with an intact and uniform NE, and the nucleoli displayed the expected crescent shape. The *mlp1Δmlp2Δ* nuclei were misshapen, with abnormal swelling of the NE luminal space and nucleoli that were frequently enlarged, and lacked cohesion and proper localization within the nucleus (Figure 10D). Finally, when preparing nuclei for EM, we found that nuclei

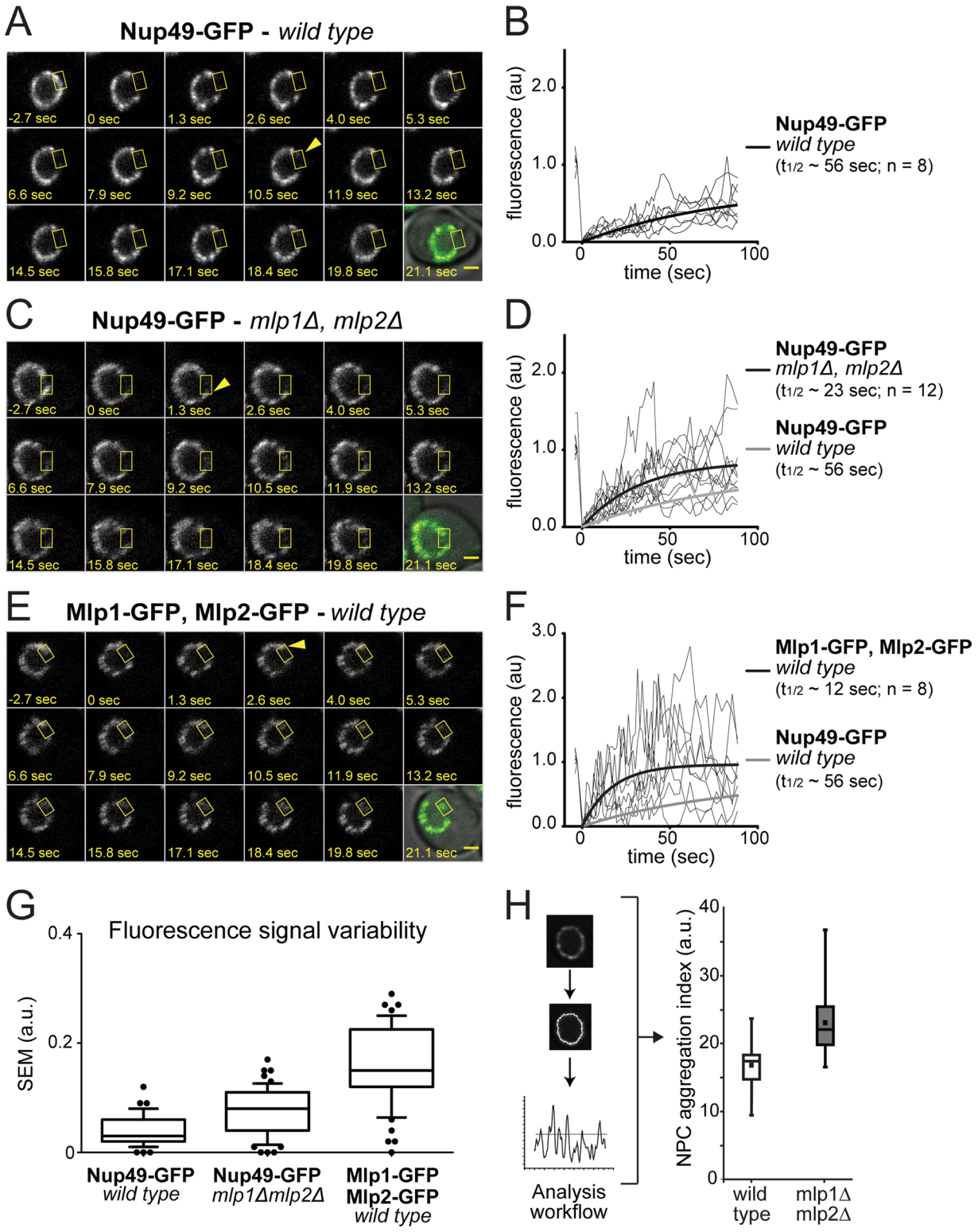

FIGURE 9: Mlps affect the mobility and distribution of NPCs in the plane of the NE. (A, C, E) Representative fluorescence microscopy images of FRAP experiments of NPCs and Mlps in wild-type cells and of NPCs in *mlp1Δmlp2Δ* cells. (B, D, F) Corresponding normalized kinetics of FRAP experiments of (B) wild-type or (D) *mlp1Δmlp2Δ* cells expressing Nup49p-GFP or of (F) wild-type cells expressing Mlp1p-GFP and Mlp2p-GFP. Recovery curves were normalized to prebleached intensity and plotted as thin traces for individual cells (Nup49p-GFP, $n = 8$; *mlp1Δmlp2Δ*, $n = 12$; Mlp1p-GFP, Mlp2p-GFP, $n = 8$). Solid lines represent an exponential regression fit based on a one-phase association equation of the mean of all cells of a given strain. (G) Box-and-whisker plots displaying the distribution of the SEM of the measured MFI for each time point, in B, D, and F ($n = 53$; $p < 0.0001$; ANOVA). (H) Schematic of method used to determine the NPC aggregation index and box-and-whisker plot of NPC aggregation index distribution in wild-type and *mlp1Δmlp2Δ* cells ($n = 50$; $p < 10^{-11}$; Student's *t* test). Bar, 2 µm (A, C, E).

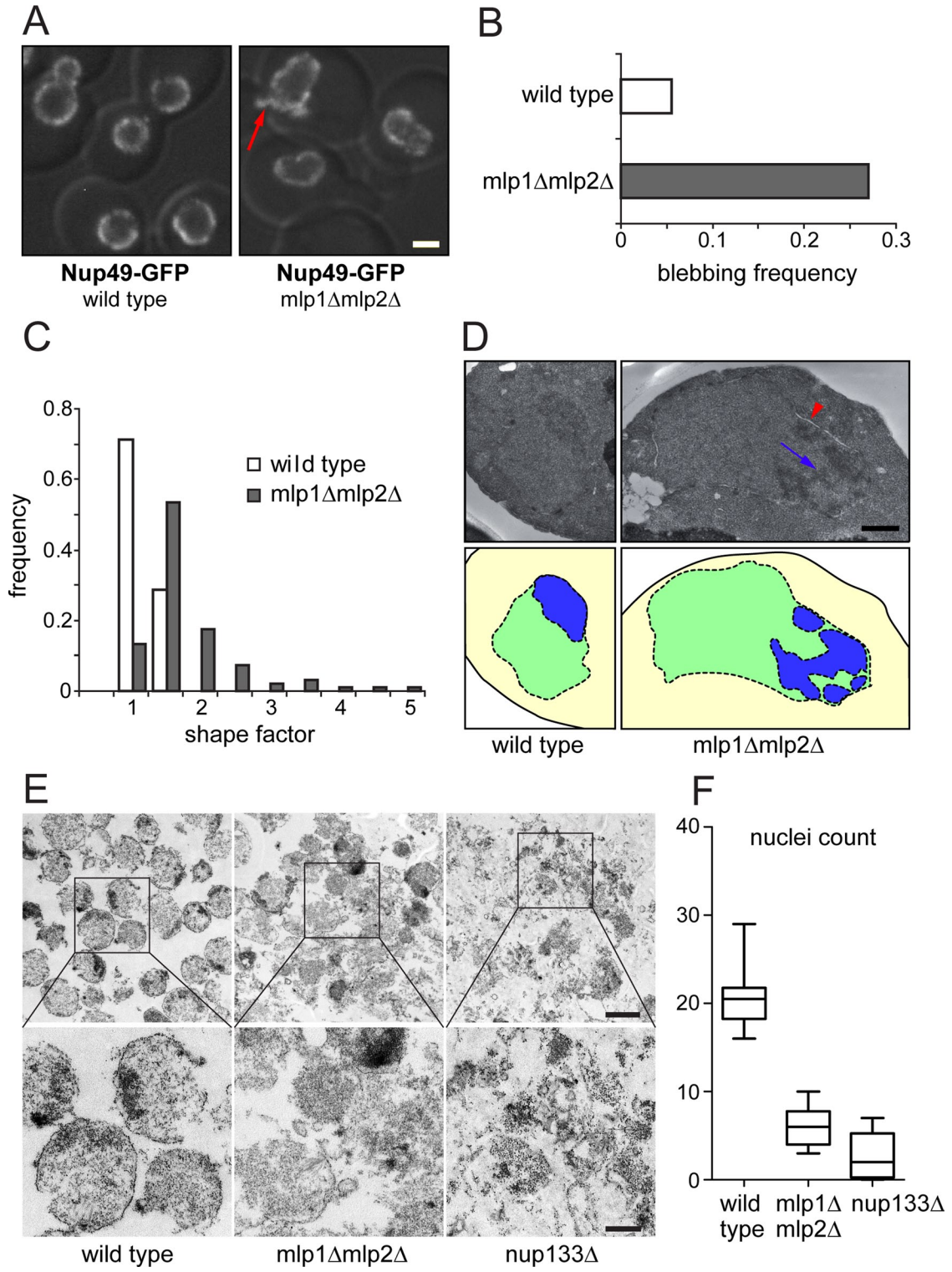

FIGURE 10: Mlps are necessary to support the physical integrity of the nuclear envelope. (A) Wild-type and *mlp1Δmlp2Δ* strains expressing Nup49p-GFP imaged by fluorescence microscopy to visualize NE morphology (red arrow indicates blebs). (B) Blebbing frequency in wild-type ($n = 380$) and *mlp1Δmlp2Δ* ($n = 461$) cells. (C) Histograms of the shape factor distribution in wild-type and *mlp1Δmlp2Δ* strains (wild type, $n = 35$; *mlp1Δmlp2Δ*, $n = 104$; $p < 0.001$; Kolmogorov–Smirnov test). (D) Thin-section TEM images (top) and graphical representations (bottom) of a wild-type (left) and *mlp1Δmlp2Δ* (right) cell identifying cytoplasm (yellow), nucleoplasm (green), and nucleolus (blue). Separated NE (red arrowhead) and abnormal nucleolus (blue arrow) are indicated. (E) Low-magnification thin-section TEM images (top) of nuclei isolated from wild-type, *mlp1Δmlp2Δ*, and *nup133Δ* cells, with high-magnification insets (bottom). (F) Frequency of intact nuclei as counted in 12 separate images of each strain shown in E ($p < 0.0001$; ANOVA). Bars, 2 µm (A), 500 nm (D), 2 µm (E, top), 0.8 µm (E, bottom).

lacking Mlps seemed much more prone to physical damage than those from wild-type cells (Figure 10E), as was anecdotally reported previously (Strambio-de-Castillia *et al.*, 1999; Hediger *et al.*, 2002). Similar behavior is seen in mutants like *nup133Δ* that drastically alter NE structure and NPC distribution, suggesting that normal NPC spacing is crucial for NE stability. We scored the number of intact nuclei across a dozen images of equal magnification and size across all three strains and found that both *mlp1Δmlp2Δ* and *nup133Δ* strains had significantly fewer intact nuclei than wild type (Figure 10F). Taken together, our data show a clear role for the Mlps in maintaining the structural integrity of the NE and its associated structures.

DISCUSSION

Mlp proteins are major NPC basket components

We show here that the Mlps are major components of the nuclear basket and necessary for its formation. Our affinity purification results indicate that the Mlps are anchored to the NPC via interactions involving Nup60p, Nup1p, the Nup84p complex, and Nic96p. This is consistent with previous findings (Feuerbach *et al.*, 2002; Galy *et al.*, 2004; Scott *et al.*, 2005; Lewis *et al.*, 2007), with the position of these Nups within the NPC structure (Rout *et al.*, 2000; Alber *et al.*, 2007b), and with human Tpr-binding Nup153, the homologue of yeast Nup1p and Nup60p (Walther *et al.*, 2001; Hase and Cordes, 2003). Simultaneous and low-affinity interactions of the Mlps with more than one Nup might explain why the Mlp's anchoring site at the NPC has proven difficult to determine. Localization of the Mlp1p N- and C-termini to NPC-associated fibrils located farther away from the NPC face than any other Nup (Rout *et al.*, 2000; Alber *et al.*, 2007b), and mapping of its NBS to a centrally located coiled-coil discontinuity suggest that the Mlps, like human Tpr (Krull *et al.*, 2004), interact with the NPC in a hairpin-like conformation extending flexible filaments up to 40 nm away from the NPC. This proposed Mlp arrangement is in good agreement with previous measurements of the yeast basket (Rout and Blobel, 1993; Kiseleva *et al.*, 2004) and is consistent with previous exhaustive surveys and mapping studies of NPC components (Rout *et al.*, 2000; Alber *et al.*, 2007b), which failed to reveal other known Nups located in correspondence with the basket's position. Finally, strains lacking Mlp proteins also lack a nuclear basket. Thus we conclude that Mlps form the key scaffold and bulk of the basket structure in budding yeast, consistent with metazoan studies on Tpr, and confirming that the Mlp and Tpr proteins, which have poor sequence homology, are in fact functional homologues.

Mlp1 and Mlp2 are not part of the core NPC structure (Strambio-de-Castillia *et al.*, 1999; Alber *et al.*, 2007b) and are associated with the NPC more transiently than core Nups, as shown by cofractionation (Strambio-de-Castillia *et al.*, 1999), IF microscopy (Strambio-de-Castillia *et al.*, 1999), affinity purification, and FRAP (present work). Consistently, they may be present in less than one copy per spoke (unpublished observations) and are absent from NPCs adjacent to the nucleolus, which implies that a large proportion of NPCs might not have any associated Mlp proteins (Galy *et al.*, 2004; Niepel *et al.*, 2005). These observations suggest that within the same cell, the structure of the basket might vary from NPC to NPC, ranging from a complete eightfold-symmetric basket to no basket at all (Tran and Wente, 2006; Raices and D'Angelo, 2012). It also suggests that the nuclear basket is far more dynamic than the NPC core and might rearrange its conformation in response to changes of the local molecular environment, as observed, for example, during large mRNP transit (Kiseleva *et al.*, 1996; Soop *et al.*, 2005).

Previous studies suggest that the basket serves as a docking site for RNPs during export (Kiseleva *et al.*, 1996; Pante *et al.*, 1997; Soop *et al.*, 2005) and aids in the organization of chromatin within the nucleus (Arlucea *et al.*, 1998; Casolari *et al.*, 2004, 2005; Cabal *et al.*, 2006; Luthra *et al.*, 2007; Tan-Wong *et al.*, 2009; Kylberg *et al.*, 2010), including the exclusion of heterochromatin from the NPC vicinity (Krull *et al.*, 2010). Our EM studies confirm that in the absence of the Mlp basket, both packed chromatin and mRNPs are located significantly closer to the NPC central transporter. This is consistent with our finding that factors involved in early steps of mRNP export and proofreading, as well as Esc1p, silencing factors, and the proteasome, are found in complex with the Mlps and the NPC (see later discussion). It therefore seems reasonable to propose that one of the roles of the nuclear basket might be to keep immature RNPs distant from the NPC transport channel and either exclude or prevent the formation of dense chromatin in the immediate vicinity of the transport channel, ensuring that NPCs remain accessible for cargoes.

The nuclear basket participates in an extended interactome at the NE

Pinpointing Mlp function has proven difficult, which might be due to the partial functional redundancy between the two proteins. However, our work shows that part of the confusion might also arise from the fact that even though the Mlps primarily appear to form the nuclear basket, they also interact with several nuclear macromolecular complexes, whose function they might influence. Our affinity purification data show that contrary to the behavior of core Nups, which appear to interact primarily with other Nups forming discrete complexes of defined stoichiometry (Alber *et al.*, 2007b), the Mlps engage in low-affinity interactions with a number of core Nups, giving rise to a molecular continuum whose connectivity is difficult to pinpoint. In addition, the Mlps physically interact, either directly or indirectly, with other nuclear factors, some of which are not directly related to NPC function. We observe here that the Mlps are linked to mRNPs via multiple essential components of the mRNA biogenesis machinery; the extended Mlp-NPC interactome is linked with silenced chromatin and the proteasome via Esc1p; and the yeast SPB is also connected to the nuclear basket via Mlp2p, which might have evolved to ensure the close tethering of the NPC to the yeast SPB required for closed mitosis (Niepel *et al.*, 2005; De Souza *et al.*, 2009). Thus it appears that the nuclear basket might represent a hub that integrates diverse macromolecular interactions occurring at the NE, presumably to ensure their close functional coupling with nuclear transport.

Esc1p exclusion from the nucleolus requires the Mlps

Previous work reported that Mlps and Esc1p have similar C-shaped distributions at the NE and are excluded from the area near the nucleolus (Galy *et al.*, 2004; Taddei *et al.*, 2004; Niepel *et al.*, 2005). Here we report that Esc1p and Mlp proteins are found in complex with each other and with the NPC and that the characteristic localization pattern of Esc1p is abolished in *mlp1Δmlp2Δ* cells. Consistently, previous reports show that deletion of *ESC1* leads to Mlp1p mislocalization (Lewis *et al.*, 2007). Our data suggest that the Esc1p–Mlp interaction is likely to be transient, indirect, and involve only a subset of Mlp molecules at any one time. The observed interdependent localization of these proteins may account for the difficulty in distinguishing the individual roles of Esc1p and the Mlp proteins in processes such as chromatin silencing (Galy *et al.*, 2000; Andrulis *et al.*, 2002; Hediger *et al.*, 2002), telomere positioning and maintenance (Feuerbach *et al.*, 2002; Hediger *et al.*, 2002; Taddei *et al.*,

2004), the regulation of SUMO conjugation (Zhao *et al.*, 2004; Palancade *et al.*, 2007), the retention and degradation of misspliced mRNA (Lewis *et al.*, 2007; Skruzný *et al.*, 2009; Iglesias *et al.*, 2010; Sayani and Chanfreau, 2012), and even maintenance of NE structure (Niepel *et al.*, 2005; Hattier *et al.*, 2007). The physical connection of the proteasome with Esc1p and their indirect interaction with the Mlps and the NPC is of particular interest, since it provides a basis for observations functionally linking the proteasome to the nuclear periphery (reviewed in Nagai *et al.*, 2011). Indeed, multiple NE-associated functions, such as sumoylation homeostasis, epigenetic rearrangement of chromatin, and degradation of malformed mRNPs, potentially require the proteasome, making its tethering to the NE functionally relevant.

The nuclear basket interactome might interconnect neighboring NPCs

EM imaging in yeast and other organisms shows that neighboring NPCs are integrated into a continuous array via protein filaments associated with the nuclear basket (Goldberg and Allen, 1992; Ris, 1997; Arlucea *et al.*, 1998; Kiseleva *et al.*, 2004, 2007). Crucially, our IEM studies indicate that Mlps not only form the basket at the NPC, but are also arranged horizontally along the plane of the NE and are found in areas bridging neighboring nuclear pores (also see Strambio-de-Castillia *et al.*, 1999). Consistently, fluorescence microscopy shows that Mlps can localize away from NPCs (Strambio-de-Castillia *et al.*, 1999; Niepel *et al.*, 2005), and upon overexpression Mlps can form a uniform dense layer at the nuclear periphery, that appears to bridge inter-NPC regions (Strambio-de-Castillia *et al.*, 1999). Affinity purification experiments, as well as purification of complexes followed by immunoblotting, and sedimentation studies (unpublished observations), demonstrate that Mlp1p and Mlp2p interact with each other and are thus capable of forming heteromultimeric and homomultimeric networks. This is consistent with previous data: a number of Mlp1p (and likely Mlp2p) molecules are associated with filaments up to 180 nm away from NPCs; Mlp1p is found in regions of the NE that do not appear to contain any NPCs; Mlp1p fails to localize exclusively to NPCs in a clustering strain; Mlp proteins fractionate differently than NPC components; and they have a localization pattern distinct from that of the NPC (Strambio-de-Castillia *et al.*, 1999; Kosova *et al.*, 2000; Niepel *et al.*, 2005). Moreover, direct attachment of Mlp2 to SPBs in the absence of Nups (Niepel *et al.*, 2005) proves that NPC-independent anchor sites for the Mlps exist at the NE. Although other possibilities cannot yet be excluded, taken together the most parsimonious explanation of these findings is that the Mlps form an extended interacting network radiating from the basket and interlinking neighboring NPCs. Further studies are clearly warranted to better define the exact role played by the Mlps at the inter-NPC regions of the NE.

Functions of a nuclear basket interaction platform

Winey *et al.* (1997) found that NPCs are regularly spaced in the plane of the NE and that a region of ~120 nm around each NPC is completely free of neighboring NPCs. Owing to their size and localization it is plausible that Mlps maintain this regular spacing and minimum distance. Indeed, we find that the absence of Mlps leads to a more random NPC placement around the NE, leading to areas with relatively higher NPC crowding alongside regions with relatively fewer NPCs. In metazoans, the NPCs are connected through the basket (Walther *et al.*, 2001) to the underlying lamina network (Daigle *et al.*, 2001; Zhou and Pante, 2010), causing their position within the NE to remain largely static. While *S. cerevisiae* has relatively more mobile NPCs (Belgareh and Doye, 1997; Bucci and Wente, 1997), we find that the Mlps considerably restrict their lateral mobility. It thus appears likely that the restricted mobility is integral to maintaining the more uniform distribution of the NPCs. Without Mlps, the NPCs are freer to diffuse along the NE and by either random chance or some other undefined mechanism, form larger clusters, which are themselves free to move along the NE and make it more likely to have areas of the NE that are relatively devoid of NPCs.

Of interest, loss of the Mlps, as well as of Nup133p (which causes more severe NPC clustering), makes the nucleus more susceptible to physical stress and breakage. The NE structure is also compromised, showing bulging and blebbing in live cells and breakage during subcellular fractionation (Strambio-de-Castillia *et al.*, 1999; Hediger *et al.*, 2002). In addition, Mlp-deficient nuclei display markedly altered nucleolar morphology, with the nucleolus losing its typical crescent shape and becoming amorphously distributed throughout the nucleus. We propose a model in which NPC–Mlp interconnections indirectly promote nuclear stability by ensuring that NPCs are uniformly distributed on the nuclear surface and can therefore act as regularly spaced "staples" clamping the two NE membranes together, making the NE less prone to blebbing and breakage and maintaining proper nucleolar–NE association.

Is an NE interaction platform a universal requirement for eukaryotes?

We propose here that NPCs are an integral part of a network of protein–protein interactions radiating from the nuclear basket. The Mlp proteins appear to be the major component of this protein network: they form the nuclear basket and might reach beyond it, linking neighboring NPCs into a molecular continuum that ensures normal NPC distribution and maintains nuclear stability (Figure 11). This interaction network appears also to serve as a hub for macromolecular structures associated with the NE, such as the SPB via Mlp2p, mRNPs caught in transit during nuclear egress via factors involved in transcription regulation and mRNA export, and silenced chromatin and the proteasome (directly or indirectly) via Esc1p. By linking the

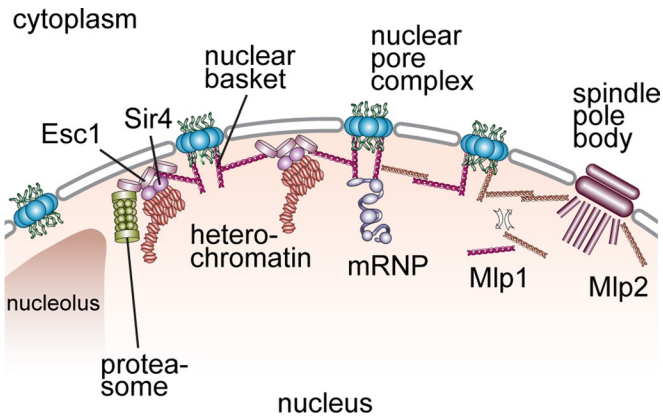

FIGURE 11: Mlp proteins form the nuclear basket and an interaction network underlying the NE. Mlp1p and Mlp2p assemble into coiled-coil dimers that form the nuclear NPC basket and extend horizontally to link adjoining NPCs. The basket serves as a site for mRNP binding, presumably facilitating mRNA proofreading, it keeps the area beneath the NPC central tube free from dense chromatin, and it might aide in the organization of these structures around the NPC. Mlps underlying the NE connect NPCs and the SPB into a network and physically support the structure of the nucleus. Esc1p is integrated into the network and anchors silenced telomeric DNA and the proteasome to the NE.

Mlps to macromolecular complexes involved in the proper function of the NPC and of the NE, our model provides an explanation for a host of observations tying the Mlps to a disparate array of seemingly unrelated nuclear processes.

Even though this yeast NE platform differs significantly from the mammalian lamina, the two structures show intriguing similarities in function. Like the Mlps, the lamins have been reported to aid in chromatin organization (reviewed in Cohen *et al.*, 2008; Andres and Gonzalez, 2009), and nuclei carrying mutations in A-type lamins show large alterations in nuclear shape, rearrangement of NPCs, and increased nuclear fragility (reviewed in Zwerger *et al.*, 2011). Affected cells are mechanically weakened, leaving them prone to damage and eventual apoptosis when exposed to mechanical stress (Lammerding *et al.*, 2004). Because yeast nuclei are protected by a strong cell wall and undergo closed mitosis, the stresses on their nuclei and requirements for assembly are reduced, and so it is not surprising that there are physical differences between the yeast NE scaffold and the mammalian lamina. Yet, their functional similarities in mechanically supporting the NE and providing an interaction platform at the nuclear periphery are striking. This suggests that an interaction platform at the NE, which helps coordinate different nuclear functions, might be a universal feature of the eukaryotic nucleus, and that in many lineages that lack the nuclear lamina, additional structural roles similar to those seen here may be played by the Tpr/Mlp network.

MATERIALS AND METHODS

Plasmids and yeast strains construction

Strains are isogenic to W303 unless otherwise specified and are described in Supplemental Table S7. Genomic tagging with fluorescent and affinity epitopes was performed as described earlier (Rout *et al.*, 2000; Niepel *et al.*, 2005). Mating, sporulation, transformation, and culturing of all yeast strains were done according to standard techniques. Details on strain construction and genotypes can be found in Supplemental Table S7. To map the NBS of Mlp1p, the pDEST-GFP-NLS vector was created by inserting the SV40 nuclear localization sequence and a Gateway reading frame cassette (Invitrogen, Carlsbad, CA) into the pUG34 vector expressing yEGFP3 (Niedenthal *et al.*, 1996). PCR products of MLP1 fragments with attB overhangs were inserted into pDONR221 (Invitrogen) and subsequently transferred to pDEST-GFP-NLS to produce expression plasmids encoding Mlp1p fragments N-terminally tagged with yEGFP3-NLS (sequences available upon request). All expression plasmids were introduced into yCS211 and grown in the presence of 150 mg/l methionine for live-cell microscopy analysis to reduce the expression level of the GFP-NLS–tagged Mlp1p fragments in target yeast cells.

Affinity purifications

Affinity purifications were performed as described previously (Niepel *et al.*, 2005; Oeffinger *et al.*, 2007) using the indicated conditions. In brief, frozen cells were ground with a motorized grinder (Retsch, Newtown, PA) and thawed into extraction buffer. Cell lysates were homogenized with a Polytron for 25 s (PT 10/35; Brinkman Instruments, Westbury, NY) and cleared. Epoxy-activated Dynabeads (M270; Invitrogen) cross-linked to rabbit immunoglobulin G (IgG; MP Biomedicals, Santa Ana, CA) were added to each lysate and incubated for 1 h at 4°C under rotation. The IgG–Dynabeads were collected with a magnet, washed five times with 1 ml of extraction buffer by gentle pipetting and once with 1 ml of 100 mM ammonium acetate, pH 7.4, and 0.1 mM $MgCl_2$ under rotation for 5 min at 25°C. The PrA-containing complexes were eluted off the beads twice with 0.5 ml of 0.5 M NH_4OH and 0.5 mM EDTA at 25°C for 20 min and lyophilized in a SpeedVac (Savant, Thermo Scientific, Waltham, MA).

Mass spectrometry

Data presented in Figure 1, A and B, and Supplemental Table S1 were obtained as described previously (Niepel *et al.*, 2005). Data presented in Figures 1, C–E, and 2 and Supplemental Tables S2–S5 were obtained as previously reported (Cristea *et al.*, 2005, 2006) with the following minor modifications. The dried pellet of isolated proteins was suspended in protein electrophoresis sample buffer, resolved by one-dimensional SDS–PAGE (NuPAGE 4–12% Bis-Tris; Invitrogen), and stained with Coomassie blue (GelCode Blue; Thermo Scientific). Each entire gel lane was cut into ~66 × 1-mm sections, and the sections were combined into ~25 samples. Each sample was digested with 125 ng of sequencing-grade modified trypsin (Promega, Madison, WI), and the resulting peptides were extracted on reverse-phase resin (Poros 20 R2; Life Technologies, Carlsbad, CA) by shaking overnight at 4°C. The samples were eluted with either 5 µl of 50% (vol/vol) methanol, 20% (vol/vol) acetonitrile, and 0.1% (vol/vol) trifluoroacetic acid, containing 1:3 vol/vol saturated 2,5-dihydroxybenzoic acid matrix solution, or 3 µl of 70% (vol/vol) acetonitrile and 0.1% (vol/vol) trifluoroacetic acid, containing 1:1 vol/vol saturated α-cyano-4-hydroxycinnamic acid matrix solution, and spotted on a matrix-assisted laser desorption/ionization (MALDI) target. Mass spectrometric analyses were carried out using MALDI MS on two different types of mass spectrometric configurations. For the wild-type Mlp1p-PrA and Mlp1p-PrA-nup1Δ samples, analyses were performed by MALDI QqTOF MS using an in-house-built MALDI interface coupled to a quadrupole Qq-TOF instrument (QqTOF Centaur; Sciex, Concorde, ON, Canada) as described (Cristea *et al.*, 2005). For the Mlp1pPrA-nup53Δ, Mlp1p-PrA-nup60Δ, Mlp1p-PrA-nup84Δ, Mlp1p-PrA-pom152Δ, Mlp1p-PrA-nup188Δ, wild-type Mlp2p-PrA, Mlp2-PrA-nup1Δ, Mlp2-PrA-nup60Δ, Mlp2-PrA-nup84Δ, and wild-type Esc1p-PrA, MALDI MS analyses were performed using prOTOF (Perkin Elmer, Waltham, MA) as described (Cristea *et al.*, 2006). Mass spectra were visualized and processed in MoverZ (Genomic Solutions, Ann Arbor, MI). For the analyses of the data generated from both mass spectrometric configurations, protein candidates were identified by database searching against the National Center for Biotechnology Information nonredundant protein database, version 06/10/16, and XProteo, which uses a Bayesian algorithm to calculate probability scores for candidate proteins (Moorman *et al.*, 2008). Search parameters for MS data were as follows: species, *S. cerevisiae* (11,105 sequences); protein mass, 0–300 kDa; protein pI, 1–14; mixture search, auto; display top, 50; enzyme, trypsin; miscleavage, 1; mass type, monoisotopic; charge state, MH+; mass tolerance, 5–50 ppm. The XProteo probability scores, based on an improved version of the ProFound Bayesian algorithm, indicated *d′* (discriminability) values for each candidate protein as the normalized distance between the score distribution (of the candidate protein) and the distribution of randomly matched proteins (in units of SD). A score of $d' = 4$ corresponded to a true-positive rate of 0.99 and a false-positive rate of 0.05.

Coimmunoprecipitation immunoblot experiments

For Mlp–Mlp interactions, cell lysates were prepared from 100 µl of yeast cell paste of each indicated strain, with their cell walls weakened by digestion with 5 mM dithiothreitol (DTT), 10% Glusulase, 0.1% Zymolyase T100, and 0.1% mutanase in 1.1 M sorbitol for 15 min at 30°C. To adjust for total protein amounts, 100 µl of untagged cell paste was added to strains marked "coexpressed." After digestion the cells were washed twice in 1.1 M sorbitol and

broken by vortexing for 5 min at 4°C with 300 µl of acid-washed glass beads in 1 ml 20 mM Na 4-(2-hydroxyethyl)-1-piperazineethanesulfonic acid (HEPES), pH 7.4, 150 mM NaCl, 0.5% Triton X-100, 1 mM DTT, 4 µg/ml pepstatin, and 0.2 mg/ml phenylmethylsulfonyl fluoride (PMSF). Lysates were cleared by centrifugation, and 2.5 mg of rabbit IgG-conjugated DynaBeads was added. Beads were incubated for 2 h at 4°C and treated as described earlier. Samples were resolved in duplicate by SDS–PAGE, and PrA- and Myc-tagged proteins were detected by immunoblotting with a 1:1000 dilution of rabbit IgG (MP Biomedicals) and an anti-Myc antibody (Santa Cruz Biotechnology, Santa Cruz, CA).

Domain analysis using protease accessibility laddering

PAL analysis was performed essentially as described previously (Dokudovskaya *et al.*, 2006). Affinity-tagged Mlp proteins were isolated as described from 0.25 g of ground yeast powder using 1× TB-T (20 mM HEPES-KOH, pH 7.4, 110 mM KOAc, 2 mM MgCl, 0.1% Tween-20 [vol/vol]), 1% Triton X, 300 mM NaCl, 1 mM DTT, 4 µg/ml pepstatin, 0.2 mg/ml PMSF and 1% Protease Inhibitor Cocktail (PIC; Sigma-Aldrich, St. Louis, MO) extraction buffer, and 2 mg of Dynabeads (Niepel *et al.*, 2005). After washing five times in 1× TB-T, 1% Triton X, and 300 mM NaCl and twice in 50 mM sodium phosphate, pH 8, and 0.01% SDS, the beads were incubated in 50 mM sodium phosphate, pH 8, and 0.01% SDS containing 1 ng/ml Asp-N (Roche, Indianapolis, IN) for the indicated length of time. Protein fragments were eluted with 0.5 M NH_4OH containing 0.5 mM EDTA, vacuum dried, resuspended in SDS–PAGE sample buffer, separated on a 4–12% Bis-Tris gel (Invitrogen), and visualized by immunoblotting.

Nuclear preparation and electron microscopy of nuclei and nuclear baskets

Nuclei were prepared from the haploid yeast strains yCS137 (wild type), yCS135 (*mlp1Δmlp2Δ*), and yCS258 (nup133Δ). Cell lysis of a spheroplast pellet from a 1-l culture was performed as described previously (Kipper *et al.*, 2002). Lysed cells were diluted in 8% PVP solution (8% [wt/vol] PVP-40, 20 mM K phosphate, pH 6.5, 7.5 µM $MgCl_2$) with 4 µg/ml pepstatin, 0.2 mg/ml PMSF, and 1% PIC to a total volume of 40 ml. A 1.875/2.5 M sucrose, Bis-Tris/Mg^{2+} (10 mM Bis-Tris, pH 6.5, 100 µM $MgCl_2$) step gradient containing 4 µg/ml pepstatin, 0.2 mg/ml PMSF, and 1% PIC was prepared in advance in two separate tubes, and the step boundary was softened through careful stirring. Lysed cells, 20 ml, were loaded onto each of the gradient-containing tubes and separated at 100,000 × *g* in a SW28 rotor for 25 min at 4°C. The nuclear fraction, found at the interface between the two steps of the gradient, was frozen in droplets using liquid nitrogen and stored at −80°C.

Isolated nuclei were incubated with 2% glutaraldehyde and 2% paraformaldehyde in 0.1 M Na cacodylate for 20 min on ice and pelleted at 40,000 × *g* in a TLA55 rotor for 30 min at 4°C, after which the supernatant was removed. The compacted pellets were fixed with 2.5% glutaraldehyde overnight at 4°C. Pellets were washed with 0.1 M Na cacodylate buffer (2 × 15 min) and postfixed with 1% osmium tetroxide containing 1% potassium ferrocyanide in cacodylate buffer for 2 h at 23°C. They were washed in distilled water (2 × 10 min), en bloc stained with 2% uranyl acetate (aq) for 1.5 h at 23°C, dehydrated in ascending ethanols, infiltrated with Spurr's resin, and polymerized for 24 h at 70°C. Sections were cut on an ultramicrotome (Ultracut E; Reichert, Depew, NY) with a diamond knife at 40- to 50-nm thickness, collected on 200 hexagonal mesh copper grids, poststained with 2% uranyl acetate (aq) and 1% lead citrate (10 min each), and imaged on a FEI Tecnai G2 Spirit Biotwin transmission electron microscope (FEI) equipped with a 4K × 4K digital camera (Gatan, Pleasanton, CA).

To differentially contrast RNA-containing structures from other structures in the cell, individual sections were stained using the well-established methodology of Bernhard (1969) and visualized as described. To quantitatively assess nuclear fragility, frequencies of intact nuclei were determined by counting, in a double-blind manner, morphologically recognizable nuclei on a total of 12 low-magnification, thin-section, Bernhard-stained TEM images obtained from yCS137, yCS135, and yCS258.

Localization of proteins by immuno electron microscopy

Samples of budding yeast strains expressing C- and N-terminally PrA-tagged Mlp proteins from the genomic copy of the gene were prepared for thin-section IEM and visualized as described previously (Rout *et al.*, 2000). The obtained images were processed, and the actual positions of both termini were estimated for both Mlp1p and Mlp2p from the distribution of their IEM labeling using a previously described method (Alber *et al.*, 2007a). In both cases, the position of both protein termini was estimated in relation to either the NPC midplane and central axis (Figure 7, A–C) or the NE midplane (Figure 7, D–F).

Live-cell microscopy and image analysis

For live imaging experiments, cells were grown and prepared for imaging as described previously (Niepel *et al.*, 2005). For the NBS mapping experiment, images of budding yeast strain yCS211 expressing Mlp1p fragments fused to the C-terminus of yEGFP3-NLS or a yEGFP3-NLS control protein (not shown) were acquired on a Nikon Eclipse E800 microscope equipped with a Nikon UR Plan Apochromat 100×/1.4 numerical aperture (NA) oil differential interference contrast (DIC) objective lens and fitted with Semrock filters (Nikon, Melville, NY). The system was controlled using OpenLab imaging software (Perkin Elmer). For NE shape and blebbing determinations, images of strains yCS374 and yCS377 were recorded using a cooled charge-coupled device camera (Orca ER; Hamamatsu, Hamamatsu, Japan) attached to a microscope (Axiovert 200; Carl Zeiss MicroImaging, Jena, Germany) fitted with a spinning disk (UltraView; Perkin Elmer) confocal imaging head and using a 100×/NA 1.45 objective lens (Plan Apochromat; Carl Zeiss MicroImaging). GFP was excited with the 488-nm line of a krypton–argon laser, using a dedicated 488-nm dichroic and standard GFP excitation/emission filters (Chroma Corp., Bellows Falls, VT). The system was controlled with MetaMorph imaging software (Molecular Devices, Sunnyvale, CA). In both cases, stacks of ten to twenty 0.22- to 0.25-µm optical sections of several fields of cells were acquired and subjected to maximum intensity projection along the optical axis. For each sample, representative nuclei were selected across at least three independent fields of view. For each nucleus, we obtained a linear plot profile of MFI along the nuclear diameter. Individual plots were normalized to the minimal MFI value and transposed along the linear dimension before averaging. Each plot represents the average of a minimum of ~20 independent nuclei. Shape factor measurements on strains yCS374 and yCS377 were determined for a statistically significant number of cells using the Morphometric Analysis module of MetaMorph. Blebbing was scored by automatically counting Nup49-GFP–positive nuclei on maximally projected image stacks obtained as described from both wild-type and *mlp1Δmlp2Δ* cells using the IdentifyPrimaryObjects module of CellProfiler, and subsequently manually scoring the presence of visible "blebs."

For FRAP experiments, strains yCS374, yMN654, and yCS377 (Figure 9) were grown as previously described (Niepel *et al.*, 2005).

To reduce cell mobility during time-lapse image acquisition, concentrated cell suspensions were spotted on 24 × 40-mm #1.5 cover slips (Fisher 12-544-C; Thermo Fisher Scientific) precoated with 1.5% low-melt agarose in growth medium. Before imaging, a second identical coverslip was layered on top, and the cells were immediately observed at room temperature (air conditioned to 23°C). Confocal images were acquired using a laser scanning confocal head (TCS SP5; Leica Microsystems, Wetzlar, Germany) fitted to the side port of an inverted microscope (DMI6000; Leica Microsystems) equipped with a Plan Apochromat 100×/1.44 NA Oil DIC objective lens (HCX PL APO CS; Leica Microsystems). GFP was excited with the 488-nm line of a multiline 100-mW argon laser (458, 476, 488, 496, 514 nm), and emitted fluorescence was detected using a HyD 2 PMT (Leica Microsystems) equipped with an acousto-optical beam splitter for emission filtering (BP 498-585; Leica Microsystems). The system was controlled using Leica LAS AF software (Leica Microsystems). FRAP experiments and MFI measurements were performed using the FRAP module of the same software. Regions of interest (ROI) were marked on areas of the NE of individual cells based on Nup49p-GFP or Mlp1p-GFP, Mlp2p-GFP labeling. One ROI was selected for bleaching for each acquisition. Two prebleaching images were recorded for normalization purposes. Bleaching was performed using the 488-nm line of the multiline argon laser at 25% intensity for a single iteration. Immediately after, a time series of ~40 individual confocal image planes was collected at ~1.33-s intervals, followed by ~15 image planes collected at ~3-s intervals to monitor the recovery of green fluorescence signal. Only time series displaying limited focal drift and overall cell displacement were selected for subsequent analysis. MFI measurements were subjected to double normalization as described previously, with minor adaptations (Phair *et al.*, 2004). Exponential regression fit calculations and significance testing were performed in GraphPad Prism 5 for Mac OS.

To measure the distribution of Esc1p-GFP (Figure 5B) and NPCs (Figure 9H) across the NE in wild-type and *mlp1Δmlp2Δ* strains, we used a DeltaVision optical sectioning microscope on a Olympus base with a 100×/1.4 NA objective and a Photometrics Cool Snap HQ camera (Applied Precision, Issaquah, WA). We used the Oval Profile Plot plug-in (http://rsbweb.nih.gov/ij/plugins/oval-profile.html) of ImageJ to create intensity profiles along the NE and determined the aggregation index, expressed as the percentage deviation from a uniform distribution and measured as the positive integral of measured intensity from the mean intensity.

Immunofluorescence microscopy

IF assays of Mlp1p-PrA and Mlp2p-PrA in wild-type and Nup deletion strains were conducted as previously described (Strambio-de-Castillia *et al.*, 1999). Images were acquired on a Nikon Eclipse E800 and a Zeiss Axioplan2 microscope, both equipped with Plan Apochromat 100×/1.4 NA oil DIC objective lenses and fitted with filters from Semrock. Acquisition was achieved using OpenLab (Perkin Elmer). Stacks of five 0.20-µm optical sections of several fields of cells were acquired, and the best focal plane for a selected image was used for presentation. IF visualization of budding yeast strains yM652 (expressing Mlp1p-GFP, Mlp2p-GFP), yMN755 (expressing Nup60p-GFP), and yMN756 (expressing Esc1p-GFP) and of yeast strain yCS211 expressing either the N-terminal 2 Mlp1p fragment fused to the C-terminus of yEGFP3-NLS or yEGP3-NLS alone as a control (Figure 6B) was performed as described (Strambio-de-Castillia *et al.*, 1999). GFP was stained with a rabbit polyclonal antibody (Cristea *et al.*, 2005), and the NPC was stained with MAb414 (Davis and Blobel, 1986). Individual confocal image planes were acquired using a TCS SP5 laser confocal head (Leica Microsystems) as described.

ACKNOWLEDGMENTS

We thank Helen Shio and Kunihiro Uryu (Rockefeller University, New York, NY) for help with the electron microscopy and Javier Fernandez-Martinez (Rockefeller University) for help with nuclei preparations. We are indebted to J. Luban (University of Massachusetts Medical School, Worcester, MA) for unwavering support and encouragement to C.S.-D.-C. throughout the course of this work. We thank O. Petrini and M. Tonolla (Istituto Cantonale di Microbiologia, Bellinzona, Switzerland) for active hospitality and support to C.-S.-D.-C. We are grateful to M. Thelen and E. Montani (Institute for Research in Biomedicine, Bellinzona, Switzerland) for assistance to C.S.-D.-C and N.V. for image acquisition. We thank P. K. Sorger (Harvard Medical School) for support of M.N. We are grateful to M. Eisenstein and T. H. Warsi for critically reviewing the manuscript and to Thoru Pederson and Reid Gilmore (University of Massachusetts Medical School) for essential encouragement and support. Funding was from the Swiss National Science Foundation (Project CRSII3_136282 to C.-S.-D.-C.), the European Commission FP7 (Project HEALTH-2007-2.3.2, GA HEALTH-F3-2008-201,032, to C.-S.-D.-C.), the National Institutes of Health (R01 GM062427, R01 GM071329, and U01 GM098256 to M.P.R.; U54 GM103511 to M.P.R. and B.T.C.; P41 GM103314 to B.T.C.; R01 GM51464 to M.N.; DP1 DA026192 and R21 AI102187 to I.M.C), and the American Cancer Society (RSG0404251 to M.P.R. and C.-S.-D.-C.). We apologize to colleagues whose work we were not able to cite due to space limitations.

REFERENCES

Alber F *et al.* (2007a). Determining the architectures of macromolecular assemblies. Nature 450, 683–694.

Alber F *et al.* (2007b). The molecular architecture of the nuclear pore complex. Nature 450, 695–701.

Andres V, Gonzalez JM (2009). Role of A-type lamins in signaling, transcription, and chromatin organization. J Cell Biol 187, 945–957.

Andrulis ED, Zappulla DC, Ansari A, Perrod S, Laiosa CV, Gartenberg MR, Sternglanz R (2002). Esc1, a nuclear periphery protein required for Sir4-based plasmid anchoring and partitioning. Mol Cell Biol 22, 8292–8301.

Arlucea J, Andrade R, Alonso R, Arechaga J (1998). The nuclear basket of the nuclear pore complex is part of a higher-order filamentous network that is related to chromatin. J Struct Biol 124, 51–58.

Bangs P, Burke B, Powers C, Craig R, Purohit A, Doxsey S (1998). Functional analysis of Tpr: identification of nuclear pore complex association and nuclear localization domains and a role in mRNA export. J Cell Biol 143, 1801–1812.

Belgareh N, Doye V (1997). Dynamics of nuclear pore distribution in nucleoporin mutant yeast cells. J Cell Biol 136, 747–759.

Bermejo R *et al.* (2011). The replication checkpoint protects fork stability by releasing transcribed genes from nuclear pores. Cell 146, 233–246.

Bermejo R, Kumar A, Foiani M (2012). Preserving the genome by regulating chromatin association with the nuclear envelope. Trends Cell Biol 22, 465–473.

Bernhard W (1969). A new staining procedure for electron microscopical cytology. J Ultrastructure Res 27, 250–265.

Bucci M, Wente SR (1997). In vivo dynamics of nuclear pore complexes in yeast. J Cell Biol 136, 1185–1199.

Cabal G *et al.* (2006). SAGA interacting factors confine sub-diffusion of transcribed genes to the nuclear envelope. Nature 441, 770–773.

Campbell JL, Lorenz A, Witkin KL, Hays T, Loidl J, Cohen-Fix O (2006). Yeast nuclear envelope subdomains with distinct abilities to resist membrane expansion. Mol Biol Cell 17, 1768–1778.

Casolari JM, Brown CR, Drubin DA, Rando OJ, Silver PA (2005). Developmentally induced changes in transcriptional program alter spatial organization across chromosomes. Genes Dev 19, 1188–1198.

Casolari JM, Brown CR, Komili S, West J, Hieronymus H, Silver PA (2004). Genome-wide localization of the nuclear transport machinery couples transcriptional status and nuclear organization. Cell 117, 427–439.

Cohen TV, Hernandez L, Stewart CL (2008). Functions of the nuclear envelope and lamina in development and disease. Biochem Soc Trans 36, 1329–1334.

Cordes VC, Reidenbach S, Rackwitz HR, Franke WW (1997). Identification of protein p270/Tpr as a constitutive component of the nuclear pore complex-attached intranuclear filaments. J Cell Biol 136, 515–529.
Cristea IM, Carroll JW, Rout MP, Rice CM, Chait BT, MacDonald MR (2006). Tracking and elucidating alphavirus-host protein interactions. J Biol Chem 281, 30269–30278.
Cristea IM, Williams R, Chait BT, Rout MP (2005). Fluorescent proteins as proteomic probes. Mol Cell Proteomics 4, 1933–1941.
Daigle N, Beaudouin J, Hartnell L, Imreh G, Hallberg E, Lippincott-Schwartz J, Ellenberg J (2001). Nuclear pore complexes form immobile networks and have a very low turnover in live mammalian cells. J Cell Biol 154, 71–84.
David-Watine B (2011). Silencing nuclear pore protein Tpr elicits a senescent-like phenotype in cancer cells. PLoS One 6, e22423.
Davis LI, Blobel G (1986). Identification and characterization of a nuclear pore complex protein. Cell 45, 699–709.
De Souza CP, Hashmi SB, Nayak T, Oakley B, Osmani SA (2009). Mlp1 acts as a mitotic scaffold to spatially regulate spindle assembly checkpoint proteins in *Aspergillus nidulans*. Mol Biol Cell 20, 2146–2159.
DeGrasse JA, DuBois KN, Devos D, Siegel TN, Sali A, Field MC, Rout MP, Chait BT (2009). Evidence for a shared nuclear pore complex architecture that is conserved from the last common eukaryotic ancestor. Mol Cell Proteomics 8, 2119–2130.
Dilworth DJ, Tackett AJ, Rogers RS, Yi EC, Christmas RH, Smith JJ, Siegel AF, Chait BT, Wozniak RW, Aitchison JD (2005). The mobile nucleoporin Nup2p and chromatin-bound Prp20p function in endogenous NPC-mediated transcriptional control. J Cell Biol 171, 955–965.
Ding D, Muthuswamy S, Meier I (2012). Functional interaction between the *Arabidopsis* orthologs of spindle assembly checkpoint proteins MAD1 and MAD2 and the nucleoporin NUA. Plant Mol Biol 79, 203–216.
Ding DQ, Tomita Y, Yamamoto A, Chikashige Y, Haraguchi T, Hiraoka Y (2000). Large-scale screening of intracellular protein localization in living fission yeast cells by the use of a GFP-fusion genomic DNA library. Genes Cells 5, 169–190.
Dokudovskaya S, Williams R, Devos D, Sali A, Chait BT, Rout MP (2006). Protease accessibility laddering: a proteomic tool for probing protein structure. Structure 14, 653–660.
Enenkel C, Lehmann A, Kloetzel PM (1998). Subcellular distribution of proteasomes implicates a major location of protein degradation in the nuclear envelope-ER network in yeast. EMBO J 17, 6144–6154.
Enenkel C, Lehmann A, Kloetzel PM (1999). GFP-labelling of 26S proteasomes in living yeast: insight into proteasomal functions at the nuclear envelope/rough ER. Mol Biol Rep 26, 131–135.
Fahrenkrog B, Hurt EC, Aebi U, Panté N (1998). Molecular architecture of the yeast nuclear pore complex: localization of Nsp1p subcomplexes. J Cell Biol 143, 577–588.
Faza MB, Kemmler S, Jimeno S, González-Aguilera C, Aguilera A, Hurt E, Panse VG (2009). Sem1 is a functional component of the nuclear pore complex-associated messenger RNA export machinery. J Cell Biol 184, 833–846.
Faza MB, Kemmler S, Panse VG (2010). Sem1: a versatile "molecular glue"? Nucleus 1, 12–17.
Feuerbach F, Galy V, Trelles-Sticken E, Fromont-Racine M, Jacquier A, Gilson E, Olivo-Marin J, Scherthan H, Nehrbass U (2002). Nuclear architecture and spatial positioning help establish transcriptional states of telomeres in yeast. Nat Cell Biol 4, 214–221.
Funasaka T, Tsuka E, Wong RW (2012). Regulation of autophagy by nucleoporin Tpr. Sci Rep 2, 878.
Galy V, Gadal O, Fromont-Racine M, Romano A, Jacquier A, Nehrbass U (2004). Nuclear retention of unspliced mRNAs in yeast is mediated by perinuclear Mlp1. Cell 116, 63–73.
Galy V, Olivo-Marin JC, Scherthan H, Doye V, Rascalou N, Nehrbass U (2000). Nuclear pore complexes in the organization of silent telomeric chromatin. Nature 403, 108–112.
Goldberg MW, Allen TD (1992). High resolution scanning electron microscopy of the nuclear envelope: demonstration of a new, regular, fibrous lattice attached to the baskets of the nucleoplasmic face of the nuclear pores. J Cell Biol 119, 1429–1440.
Green DM, Johnson CP, Hagan H, Corbett AH (2003). The C-terminal domain of myosin-like protein 1 (Mlp1p) is a docking site for heterogeneous nuclear ribonucleoproteins that are required for mRNA export. Proc Natl Acad Sci USA 100, 1010–1015.
Hase ME, Cordes VC (2003). Direct interaction with nup153 mediates binding of Tpr to the periphery of the nuclear pore complex. Mol Biol Cell 14, 1923–1940.
Hase ME, Kuznetsov NV, Cordes VC (2001). Amino acid substitutions of coiled-coil protein Tpr abrogate anchorage to the nuclear pore complex but not parallel, in-register homodimerization. Mol Biol Cell 12, 2433–2452.
Hattier T, Andrulis ED, Tartakoff AM (2007). Immobility, inheritance and plasticity of shape of the yeast nucleus. BMC Cell Biol 8, 47.
Hediger F, Dubrana K, Gasser S (2002). Myosin-like proteins 1 and 2 are not required for silencing or telomere anchoring, but act in the Tel1 pathway of telomere length control. J Struct Biol 140, 79–91.
Iglesias N, Tutucci E, Gwizdek C, Vinciguerra P, Von Dach E, Corbett AH, Dargemont C, Stutz F (2010). Ubiquitin-mediated mRNP dynamics and surveillance prior to budding yeast mRNA export. Genes Dev 24, 1927–1938.
Ishii K, Arib G, Lin C, Van Houwe G, Laemmli UK (2002). Chromatin boundaries in budding yeast: the nuclear pore connection. Cell 109, 551–562.
Jani D, Lutz S, Hurt E, Laskey RA, Stewart M, Wickramasinghe VO (2012). Functional and structural characterization of the mammalian TREX-2 complex that links transcription with nuclear messenger RNA export. Nucleic Acids Res 40, 4562–4573.
Jarnik M, Aebi U (1991). Toward a more complete 3-D structure of the nuclear pore complex. J Struct Biol 107, 291–308.
Kalkum M, Lyon GJ, Chait BT (2003). Detection of secreted peptides by using hypothesis-driven multistage mass spectrometry. Proc Natl Acad Sci USA 100, 2795–2800.
Kipper J, Strambio-de-Castillia C, Suprapto A, Rout MP (2002). Isolation of nuclear envelope from *Saccharomyces cerevisiae*. Methods Enzymol 351, 394–408.
Kiseleva E, Allen TD, Rutherford SA, Bucci M, Wente SR, Goldberg MW (2004). Yeast nuclear pore complexes have a cytoplasmic ring and internal filaments. J Struct Biol 145, 272–288.
Kiseleva E, Allen TD, Rutherford SA, Murray S, Morozova K, Gardiner F, Goldberg MW, Drummond SP (2007). A protocol for isolation and visualization of yeast nuclei by scanning electron microscopy (SEM). Nat Protoc 2, 1943–1953.
Kiseleva E, Goldberg MW, Allen TD, Akey CW (1998). Active nuclear pore complexes in *Chironomus*: visualization of transporter configurations related to mRNP export. J. Cell Sci. 111 (Pt 2), 223–236.
Kiseleva E, Goldberg MW, Daneholt B, Allen TD (1996). RNP export is mediated by structural reorganization of the nuclear pore basket. J Mol Biol 260, 304–311.
Kölling R, Nguyen T, Chen EY, Botstein D (1993). A new yeast gene with a myosin-like heptad repeat structure. Mol Gen Genet 237, 359–369.
Kosova B, Panté N, Rollenhagen C, Podtelejnikov A, Mann M, Aebi U, Hurt EC (2000). Mlp2p, a component of nuclear pore attached intranuclear filaments, associates with nic96p. J Biol Chem 275, 343–350.
Krogan NJ *et al.* (2004). Proteasome involvement in the repair of DNA double-strand breaks. Mol Cell 16, 1027–1034.
Krull S, Dorries J, Boysen B, Reidenbach S, Magnius L, Norder H, Thyberg J, Cordes VC (2010). Protein Tpr is required for establishing nuclear pore-associated zones of heterochromatin exclusion. EMBO J 29, 1659–1673.
Krull S, Thyberg J, Björkroth B, Rackwitz HR, Cordes VC (2004). Nucleoporins as components of the nuclear pore complex core structure and Tpr as the architectural element of the nuclear basket. Mol Biol Cell 15, 4261–4277.
Kuznetsov NV, Sandblad L, Hase ME, Hunziker A, Hergt M, Cordes VC (2002). The evolutionarily conserved single-copy gene for murine Tpr encodes one prevalent isoform in somatic cells and lacks paralogs in higher eukaryotes. Chromosoma 111, 236–255.
Kylberg K, Bjork P, Fomproix N, Ivarsson B, Wieslander L, Daneholt B (2010). Exclusion of mRNPs and ribosomal particles from a thin zone beneath the nuclear envelope revealed upon inhibition of transport. Exp Cell Res 316, 1028–1038.
Lammerding J, Schulze PC, Takahashi T, Kozlov S, Sullivan T, Kamm RD, Stewart CL, Lee RT (2004). Lamin A/C deficiency causes defective nuclear mechanics and mechanotransduction. J Clin Invest 113, 370–378.
Lewis A, Felberbaum R, Hochstrasser M (2007). A nuclear envelope protein linking nuclear pore basket assembly, SUMO protease regulation, and mRNA surveillance. J Cell Biol 178, 813–827.
Lince-Faria M, Maffini S, Orr B, Ding Y, Claudia F, Sunkel CE, Tavares A, Johansen J, Johansen KM, Maiato H (2009). Spatiotemporal control of mitosis by the conserved spindle matrix protein Megator. J Cell Biol 184, 647–657.
Lupas A (1997). Predicting coiled-coil regions in proteins. Curr Opin Struct Biol 7, 388–393.
Luthra R, Kerr SC, Harreman MT, Apponi LH, Fasken MB, Ramineni S, Chaurasia S, Valentini SR, Corbett AH (2007). Actively transcribed GAL

genes can be physically linked to the nuclear pore by the SAGA chromatin modifying complex. J Biol Chem 282, 3042–3049.
Moorman NJ, Cristea IM, Terhune SS, Rout MP, Chait BT, Shenk T (2008). Human cytomegalovirus protein UL38 inhibits host cell stress responses by antagonizing the tuberous sclerosis protein complex. Cell Host Microbe 3, 253–262.
Nagai S, Davoodi N, Gasser SM (2011). Nuclear organization in genome stability: SUMO connections. Cell Res 21, 474–485.
Nakano H, Funasaka T, Hashizume C, Wong RW (2010). Nucleoporin translocated promoter region (Tpr) associates with dynein complex, preventing chromosome lagging formation during mitosis. J Biol Chem 285, 10841–10849.
Niedenthal RK, Riles L, Johnston M, Hegemann JH (1996). Green fluorescent protein as a marker for gene expression and subcellular localization in budding yeast. Yeast 12, 773–786.
Niepel M, Strambio-de-Castillia C, Fasolo J, Chait BT, Rout MP (2005). The nuclear pore complex-associated protein, Mlp2p, binds to the yeast spindle pole body and promotes its efficient assembly. J Cell Biol 170, 225–235.
Oeffinger M, Wei KE, Rogers R, DeGrasse JA, Chait BT, Aitchison JD, Rout MP (2007). Comprehensive analysis of diverse ribonucleoprotein complexes. Nat Methods 4, 951–956.
Palancade B, Liu X, Garcia-Rubio M, Aguilera A, Zhao X, Doye V (2007). Nucleoporins prevent DNA damage accumulation by modulating Ulp1-dependent sumoylation processes. Mol Biol Cell 18, 2912–2923.
Palancade B, Zuccolo M, Loeillet S, Nicolas A, Doye V (2005). Pml39, a novel protein of the nuclear periphery required for nuclear retention of improper messenger ribonucleoparticles. Mol Biol Cell 16, 5258–5268.
Pante N, Jarmolowski A, Izaurralde E, Sauder U, Baschong W, Mattaj IW (1997). Visualizing nuclear export of different classes of RNA by electron microscopy. RNA 3, 498–513.
Pasupala N, Easwaran S, Hannan A, Shore D, Mishra K (2012). The SUMO E3 ligase Siz2 exerts a locus-dependent effect on gene silencing in *Saccharomyces cerevisiae*. Eukaryot Cell 11, 452–462.
Phair RD, Gorski SA, Misteli T (2004). Measurement of dynamic protein binding to chromatin in vivo, using photobleaching microscopy. Methods Enzymol 375, 393–414.
Raices M, D'Angelo MA (2012). Nuclear pore complex composition: a new regulator of tissue-specific and developmental functions. Nat Rev Mol Cell Biol 13, 687–699.
Rajanala K, Nandicoori VK (2012). Localization of nucleoporin Tpr to the nuclear pore complex is essential for Tpr mediated regulation of the export of unspliced RNA. PLoS One 7, e29921.
Ris H (1997). High-resolution field-emission scanning electron microscopy of nuclear pore complex. Scanning 19, 368–375.
Rout MP, Aitchison JD, Suprapto A, Hjertaas K, Zhao Y, Chait BT (2000). The yeast nuclear pore complex: composition, architecture, and transport mechanism. J Cell Biol 148, 635–651.
Rout MP, Blobel G (1993). Isolation of the yeast nuclear pore complex. J Cell Biol 123, 771–783.
Saguez C, Schmid M, Olesen JR, Ghazy MA, Qu X, Poulsen MB, Nasser T, Moore C, Jensen TH (2008). Nuclear mRNA surveillance in THO/sub2 mutants is triggered by inefficient polyadenylation. Mol Cell 31, 91–103.
Sayani S, Chanfreau GF (2012). Sequential RNA degradation pathways provide a fail-safe mechanism to limit the accumulation of unspliced transcripts in *Saccharomyces cerevisiae*. RNA 18, 1563–1572.
Scott RJ, Lusk CP, Dilworth DJ, Aitchison JD, Wozniak RW (2005). Interactions between Mad1p and the nuclear transport machinery in the yeast *Saccharomyces cerevisiae*. Mol Biol Cell 16, 4362–4374.
Skruzný M, Schneider C, Rácz A, Weng J, Tollervey D, Hurt E (2009). An endoribonuclease functionally linked to perinuclear mRNP quality control associates with the nuclear pore complexes. PLoS Biol 7, e8.
Soop T, Ivarsson B, Björkroth B, Fomproix N, Masich S, Cordes VC, Daneholt B (2005). Nup153 affects entry of messenger and ribosomal ribonucleoproteins into the nuclear basket during export. Mol Biol Cell 16, 5610–5620.
Strambio-de-Castillia C, Blobel G, Rout MP (1999). Proteins connecting the nuclear pore complex with the nuclear interior. J Cell Biol 144, 839–855.
Strambio-De-Castillia C, Niepel M, Rout MP (2010). The nuclear pore complex: bridging nuclear transport and gene regulation. Nat Rev Mol Cell Biol 11, 490–501.
Taddei A, Hediger F, Neumann FR, Bauer C, Gasser S (2004). Separation of silencing from perinuclear anchoring functions in yeast Ku80, Sir4 and Esc1 proteins. EMBO J 23, 1301–1312.
Taddei A, Van Houwe G, Hediger F, Kalck V, Cubizolles F, Schober H, Gasser S (2006). Nuclear pore association confers optimal expression levels for an inducible yeast gene. Nature 441, 774–778.
Tan-Wong SM, Wijayatilake HD, Proudfoot NJ (2009). Gene loops function to maintain transcriptional memory through interaction with the nuclear pore complex. Genes Dev 23, 2610–2624.
Titus LC, Dawson TR, Rexer DJ, Ryan KJ, Wente SR (2010). Members of the RSC chromatin-remodeling complex are required for maintaining proper nuclear envelope structure and pore complex localization. Mol Biol Cell 21, 1072–1087.
Tran EJ, Wente SR (2006). Dynamic nuclear pore complexes: life on the edge. Cell 125, 1041–1053.
Vaquerizas JM, Suyama R, Kind J, Miura K, Luscombe NM, Akhtar A (2010). Nuclear pore proteins nup153 and megator define transcriptionally active regions in the *Drosophila* genome. PLoS Genet 6, e1000846.
Vinciguerra P, Iglesias N, Camblong J, Zenklusen D, Stutz F (2005). Perinuclear Mlp proteins downregulate gene expression in response to a defect in mRNA export. EMBO J 24, 813–823.
Walther TC, Fornerod M, Pickersgill H, Goldberg M, Allen TD, Mattaj IW (2001). The nucleoporin Nup153 is required for nuclear pore basket formation, nuclear pore complex anchoring and import of a subset of nuclear proteins. EMBO J 20, 5703–5714.
Wente SR, Blobel G (1994). NUP145 encodes a novel yeast glycine-leucine-phenylalanine-glycine (GLFG) nucleoporin required for nuclear envelope structure. J Cell Biol 125, 955–969.
Wilmes GM *et al.* (2008). A genetic interaction map of RNA-processing factors reveals links between Sem1/Dss1-containing complexes and mRNA export and splicing. Mol Cell 32, 735–746.
Winey M, Yarar D, Giddings TH Jr, Mastronarde DN (1997). Nuclear pore complex number and distribution throughout the *Saccharomyces cerevisiae* cell cycle by three-dimensional reconstruction from electron micrographs of nuclear envelopes. Mol Biol Cell 8, 2119–2132.
Witkin KL, Friederichs JM, Cohen-Fix O, Jaspersen SL (2010). Changes in the nuclear envelope environment affect spindle pole body duplication in *Saccharomyces cerevisiae*. Genetics 186, 867–883.
Wolf DH, Hilt W (2004). The proteasome: a proteolytic nanomachine of cell regulation and waste disposal. Biochim Biophys Acta 1695, 19–31.
Xu XM, Rose A, Muthuswamy S, Jeong SY, Venkatakrishnan S, Zhao Q, Meier I (2007). Nuclear Pore Anchor, the *Arabidopsis* homolog of Tpr/Mlp1/Mlp2/megator, is involved in mRNA export and SUMO homeostasis and affects diverse aspects of plant development. Plant Cell 19, 1537–1548.
Yewdell WT, Colombi P, Makhnevych T, Lusk CP (2011). Lumenal interactions in nuclear pore complex assembly and stability. Mol Biol Cell 22, 1375–1388.
Zhao X, Wu CY, Blobel G (2004). Mlp-dependent anchorage and stabilization of a desumoylating enzyme is required to prevent clonal lethality. J Cell Biol 167, 605–611.
Zhou L, Pante N (2010). The nucleoporin Nup153 maintains nuclear envelope architecture and is required for cell migration in tumor cells. FEBS Lett 584, 3013–3020.
Zwerger M, Ho CY, Lammerding J (2011). Nuclear mechanics in disease. Annu Rev Biomed Eng 13, 397–428.